PET Evaluation of Lung Cancer*

Tira Bunyaviroch, MD[1]; and R. Edward Coleman, MD[2]

[1]Boston University School of Medicine and Boston Medical Center, Boston, Massachusetts; and [2]Duke University Medical Center, Durham, North Carolina

In the last hundred years, lung cancer has risen from a reportable disease to the most common cause of death from cancer in both men and women in developed countries (*1*). When descriptions of lung cancer were published in 1912, there were only 374 reported cases (*2*). In the 1950s, little more than the chest radiograph and sputum cytologic analysis were available for lung cancer screening. Since then, the mortality from lung cancer has decreased, but the 5-y cure rates have barely improved (*1*). The annual number of deaths from lung cancer is greater than the numbers of deaths from breast, colon, and prostate cancers combined. More than 150,000 patients died of lung cancer in 2004. The 5-y survival rates currently are 16% in the United States and 5% in the United Kingdom. The association of lung cancer with tobacco smoking was initially reported in the 1950s (*3*) and subsequently led to the determination by the U.S. Surgeon General that smoking is harmful to one's health (*4*). Further investigation has led to the discovery that this association is related to the type and amount of tobacco product used, the age at initiation, and the duration of use.

Lung cancer often presents as a solitary pulmonary nodule on chest radiographs. Chest radiographs usually are performed for patients as a preoperative or physical examination screening test, often in the absence of symptoms. Few signs and symptoms are present at an early stage, leading to more advanced disease when patients present to their physicians. One third of lung nodules in patients more than 35 y old are found to be malignant. Over 50% of the radiographically indeterminate nodules resected at thoracoscopy are benign (*5*). It is clear that there is a need for the accurate diagnosis of these lesions. The use of PET has much promise as an aid to the noninvasive evaluation of lung cancer. ^{18}F-FDG PET currently is indicated for the characterization of lung lesions, staging of non–small cell lung carcinoma (NSCLC), detection of distant metastases, and diagnosis of recurrent disease. Furthermore, many institutions have found significant value in ^{18}F-FDG PET for treatment monitoring (*6–8*).

Received Nov. 1, 2005; revision accepted Jan. 20, 2006.

For correspondence or reprints contact: R. Edward Coleman, MD, Nuclear Medicine Section, Department of Radiology, Duke University Medical Center, Durham, NC 27710.

E-mail: colem010@mc.duke.edu

*NOTE: FOR CE CREDIT, YOU CAN ACCESS THIS ACTIVITY THROUGH THE SNM WEB SITE (http://www.snm.org/ce_online) THROUGH MARCH 2007.

CONVENTIONAL IMAGING OF LUNG NODULES

The definition of a solitary pulmonary nodule is an opacity in the lung parenchyma that measures up to 3 cm and that has no associated mediastinal adenopathy or atelectasis. Lesions measuring greater than 3 cm are classified as masses (*9*). Lung nodules can be benign or malignant and can have a multitude of causes, ranging from inflammatory and infectious etiologies to malignancies. The morphologic characteristics revealed by chest radiographs and CT provide much information to aid in the diagnosis of a nodule. ^{18}F-FDG PET provides complementary information on the metabolic activity of a nodule that cannot be obtained by radiographic methods and that otherwise can be inferred only over time.

The evaluation of a solitary pulmonary nodule often begins when it is discovered incidentally on a chest radiograph, prompting further workup. Additional evaluation may reveal characteristics that indicate benignity or that warrant follow-up or biopsy. A nodule newly discovered on a chest radiograph should be analyzed for benign characteristics. A uniformly and densely calcified rounded nodule on a chest radiograph is classified easily as benign. Few nodules can be determined to be benign on the basis of chest radiographic findings, and most cases are referred for CT evaluation. Radiographs obtained before CT are invaluable for determining the time course of the development of a nodule. Subtle changes are not well evaluated on chest radiographs, but finding little change in appearance over 2 y or, preferably, longer would be more convincing of benignity.

Before the advent of PET, an indeterminate nodule on a chest radiograph was best evaluated initially with CT (*10,11*). CT remains an integral part of the evaluation of solitary pulmonary nodules; however, more options are now available to clinicians for evaluating such nodules. CT is used to evaluate the shapes, borders, and densities of nodules. CT densitometry has been used to detect calcifications within nodules. Although internal calcifications in general are frequently associated with benignity, calcified lung nodules also may result from metastasis from primary bone tumors,

soft-tissue sarcomas, and mucin-producing adenocarcinomas. In addition, internal hemorrhage, such as that which occurs within choriocarcinoma and melanoma metastases, can simulate the increased density of calcifications. Diffuse calcifications measuring greater than 300 Hounsfield units (HU) throughout a nodule are indicative of a benign nodule. A well-circumscribed nodule with central or lamellar calcifications also is indicative of benignity (*9*). The diagnosis of a benign nodule is presumed only when a majority of the lesion demonstrates attenuation consistent with calcium. The calcifications must be located in the center of the lesion to be considered benign. Other patterns include popcorn or chondroid calcifications, which, in conjunction with fat, are characteristic of hamartomas. Figures 1 and 2 demonstrate shapes, borders, and patterns of calcification in pulmonary nodules. In addition, the pattern of contrast enhancement can indicate benignity. A nodule that enhances at less than 15 HU in its central portion is considered benign. A nodule with enhancement at greater than 25 HU is considered malignant (*12,13*). The use of contrast enhancement to characterize pulmonary nodules as benign or malignant has not gained widespread acceptance.

Ground-glass opacities also can have a nodular appearance. Ground-glass nodules are less dense than solid nodules and the surrounding pulmonary vasculature and do not obscure the lung parenchyma (Fig. 3). These nodules also are referred to as subsolid nodules and can be purely ground-glass in appearance or can have mixed solid and ground-glass components. Ground-glass opacities continue to be a dilemma, as the morphologic characteristics of a benign or malignant ground-glass nodule are less well described.

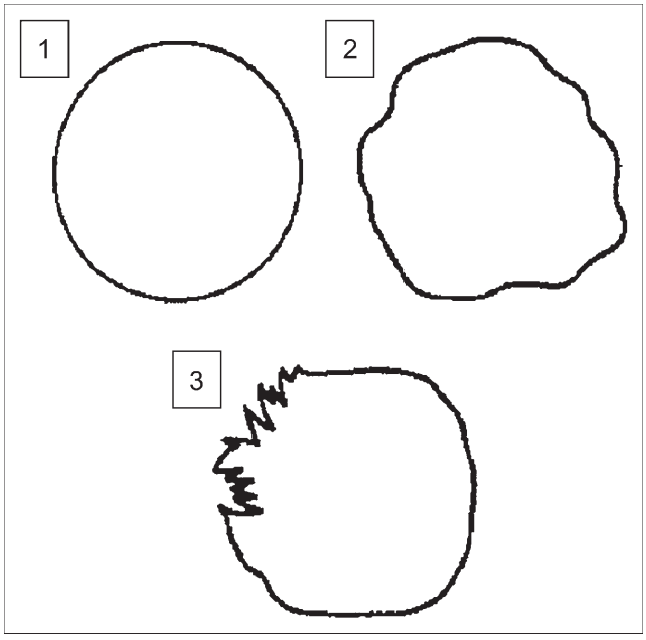

FIGURE 1. Schematic diagram of pulmonary nodules. Nodule 1 has smooth, well-defined border. Nodule 2 has lobulated border. Nodule 3 has spiculated border. (Reprinted with permission of (*9*).)

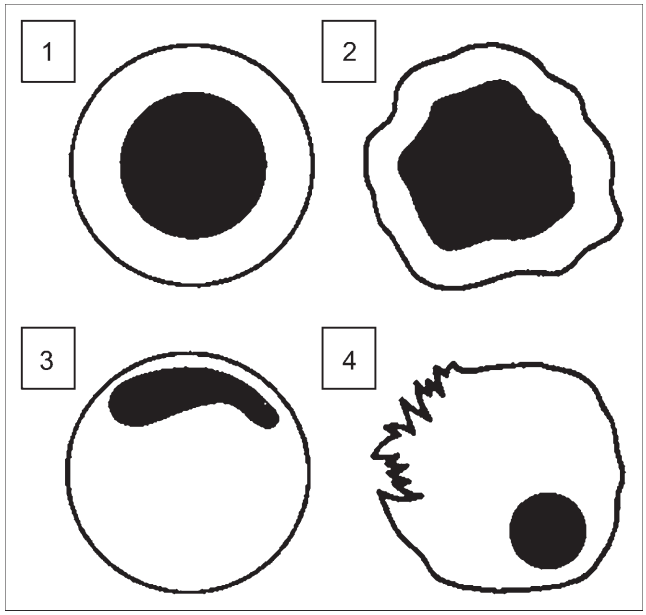

FIGURE 2. Patterns of calcification in pulmonary nodules. Nodules 1 and 2 have central calcifications, a benign pattern. Nodules 3 and 4 have eccentric calcifications, which cannot be classified as benign. (Reprinted with permission of (*9*).)

According to the Early Lung Cancer Action Program (ELCAP) study, 20% of pulmonary nodules on baseline screening are ground-glass or subsolid (*14*). That study demonstrated that the overall frequency of malignancy is much higher in ground-glass and mixed nodules than in solid nodules. The cell types of malignancies within these nodules also are different from those within solid nodules. The cell types typically included pure bronchioalveolar cells or adenocarcinomas with bronchioalveolar features. Solid nodules are typically invasive subtypes of adenocarcinoma. There are few data on the evaluation of ground-glass nodules by ^{18}F-FDG PET. One source reported a sensitivity of 10% and a specificity of 20% for ground-glass nodules on ^{18}F-FDG PET (*15*). Further investigation is necessary; however, the pathology findings of the ELCAP study suggest that there will be little utility in the diagnosis or follow-up of ground-glass nodules by ^{18}F-FDG PET because of the small size of the nodules and the potential for false-negative findings in focal bronchioalveolar cell carcinoma.

Certain morphologic characteristics of pulmonary nodules are considered indicative of malignancy; these include a spiculated outer margin (Fig. 1), a hazy and indistinct margin, endobronchial extension, extension to pulmonary veins, and focal retraction of the adjacent pleura. Heterogeneous internal composition and associated necrosis are indicative of malignancy. Malignant lesions also can simulate benign conditions by creating air bronchograms that are commonly associated with pneumonia. Entities such as bronchioalveolar cell carcinoma and lymphoma can masquerade as benign lung lesions.

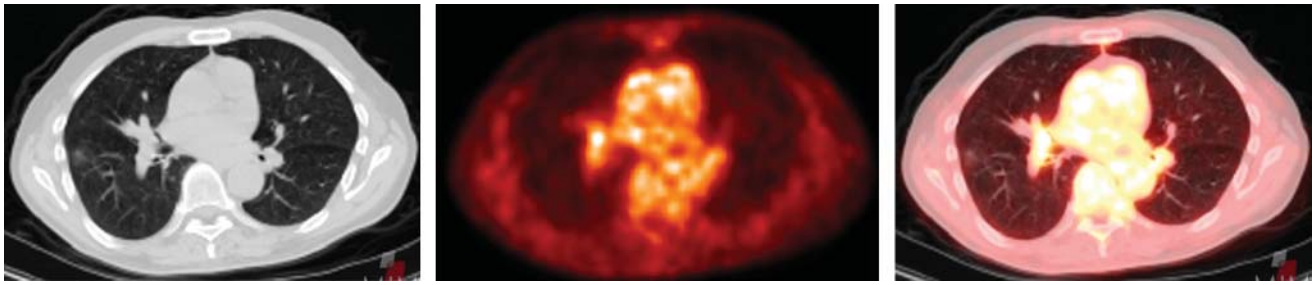

FIGURE 3. Ground-glass opacity in peripheral right lung. Mild ^{18}F-FDG activity is associated with this lesion.

Malignant nodules are not always easily distinguished from benign nodules. Furthermore, 25%−39% of malignant nodules are inaccurately classified as benign after radiologic assessment of morphologic characteristics, including size, margins, contour, and internal characteristics (*16*). Morphologic stability over 2 y is considered a reliable sign of benignity. The doubling time of the volume of a nodule is a commonly used marker of the growth of the nodule. For malignant nodules, the doubling time is usually 30–400 d. Benign nodules demonstrate doubling times outside this range, both higher and lower. Because a doubling in volume amounts to a 26% increase in nodule diameter (*17*), a significant change in nodule size may be difficult to appreciate, especially for a small nodule. Furthermore, the predictive value of stability in size may be only 65% (*18*).

Clinical information often is useful in the assessment of pulmonary nodules. Important features of the patient's history can be combined with imaging findings to calculate a likelihood ratio for malignant disease (Table 1). This type of Bayesian analysis can be used to stratify the patient's risk of malignancy and to guide management. In this scheme, patients are monitored if the probability of cancer is less than 5%, the lesion is biopsied if the probability is between 5% and 60%, and nodules are resected if the probability is greater than 60% (*19,20*). About half of the patients undergoing surgical biopsy of an indeterminate pulmonary nodule have benign disease (*5,21*).

TABLE 1
Likelihood Ratios for Lung Cancer, as Determined by Morphologic and Demographic Information

Feature or characteristic	Likelihood ratio
Spiculated margin	5.54
Lesion > 3 cm	5.23
Subject > 70 y old	4.16
Malignant growth rate	3.40
Subject smokes tobacco	2.27
Upper-lobe nodule	1.22
Lesion < 1 cm	0.52
Smooth margins	0.30
Subject 30–39 y old	0.24
Subject never smoked	0.19
Subject 20–29 y old	0.05
Benign calcification	0.01
Benign growth rate	0.01

Reprinted with permission of (*16*).

^{18}F-FDG PET FOR EVALUATION OF SOLITARY PULMONARY NODULES

The development of ^{18}F-FDG PET has taken the evaluation of solitary pulmonary nodules beyond morphologic and predictive analyses to functional and metabolic analyses of disease. PET alone has been described as a better predictor of malignancy than clinical and morphologic criteria combined (*22,23*). A prospective study of 87 patients examined whether preferential ^{18}F-FDG uptake in malignant nodules could differentiate these from benign pulmonary nodules (*24*). The investigators found that when a mean standardized uptake value (SUV) of greater than or equal to 2.5 was used for detecting malignancy, the sensitivity, specificity, and accuracy were 97%, 82%, and 92%, respectively (Fig. 4). In addition, they also determined that there was a significant correlation between the doubling time of tumor volume and the SUV. Subsequent studies demonstrated a sensitivity of 90%−100% and specificity of 69%−95% for PET (*15,25,26*). Although the SUV is a useful tool, it has been shown to be equivalent to the visual estimate of metabolic activity by experienced physicians (*27,28*).

Studies that favor ^{18}F-FDG PET for the diagnostic workup of solitary pulmonary nodules to reduce inappropriate invasive diagnostic investigation and subsequent complications are emerging. A study performed in Italy compared the traditional workup of a solitary pulmonary nodule with CT, fine-needle aspiration, and thoracoscopic biopsy with a diagnostic workup including ^{18}F-FDG PET (*29*). That study demonstrated a cost reduction of approximately €50 (~$60) per patient when PET was added to the traditional workup. A recent study in France compared the cost-effectiveness ratios of 3 management scenarios for solitary pulmonary nodules: wait and watch with periodic CT, PET, and CT plus PET (*30*). For their typical patient, a 65-y-old male smoker with a 2-cm solitary pulmonary nodule and an associated high risk of malignancy of 43%, the wait-and-watch scenario was the least effective strategy. CT plus PET was the most effective strategy and had a lower incremental cost-effectiveness ratio. Their conclusion was that

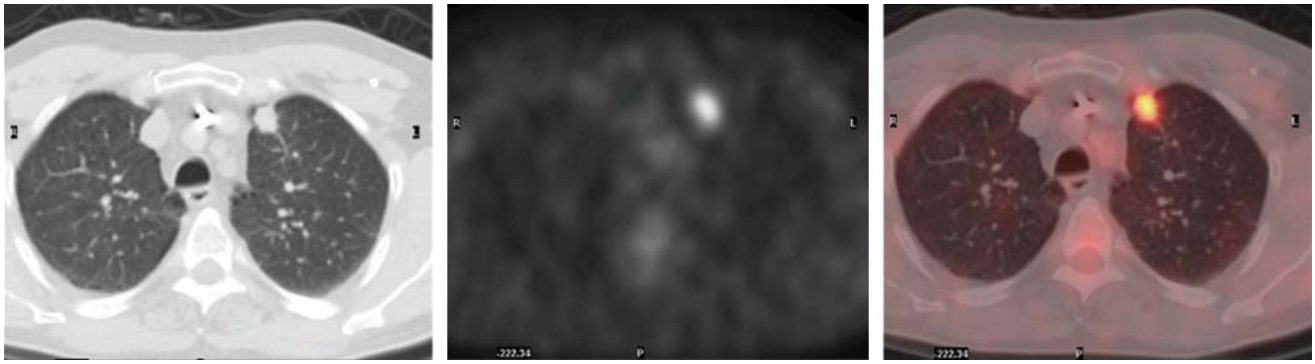

FIGURE 4. Solitary pulmonary nodule with spiculated borders in left upper lobe. No mediastinal adenopathy was present on additional images. Hypermetabolism is present within this nodule. Maximum SUV measures 6.7 g/mL. Findings are consistent with malignancy.

CT plus PET was the most cost-effective strategy for patients with a risk of malignancy of 5.7%−87%. The wait-and-watch scenario was most cost-effective for patients with a risk of 0.3%−5%.

The minimum size of a pulmonary nodule has been an issue with regard to accurate diagnostic evaluation, follow-up, and even biopsy. The NY-ELCAP study monitored 378 patients with pulmonary nodules determined by CT to be less than 5 mm in diameter. None of these nodules was diagnosed as pathologically malignant, leading the researchers to suggest limiting further workup to nodules that were 5 mm or larger (*31*). A group in Spain investigated the utility of PET in evaluating nodules of 5–10 mm in diameter and greater than 10 mm in diameter; the sensitivity for detecting malignancy in all nodules was fairly low, at 69%, whereas the sensitivity for detecting malignancy in nodules of greater than 10 mm was 95% (*32*). The authors noted that the apparent uptake in nodules decreased when the diameter was less than twice the spatial resolution of the system (approximately 7−8 mm); thus, different criteria are needed to determine malignancy in nodules of less than 15 mm. Short-term follow-up of 5- to 10-mm nodules with CT alone to evaluate for growth resulted in a low rate of invasive procedures for benign nodules. In a phantom study with ^{18}F-FDG-filled spheres measuring between 6 and 22 mm, the detection of nodules of less than 7 mm was unreliable (*33*). Further investigation is necessary to determine the best method for evaluating subcentimeter nodules.

Dual-time-point imaging has emerged as a potential discriminator of benign and malignant diseases, with images being obtained at 1 and 2 h after the administration of ^{18}F-FDG. In a study involving in vitro samples and animal and human subjects, ^{18}F-FDG uptake was measured over time; Zhuang et al. found that malignant lesions showed a significant increase in SUV over time and that benign lesions showed a decrease over time (*34*). Additional investigation has reached similar conclusions (*35*). One study compared single-time-point imaging and dual-time-point imaging with a cutoff SUV of 2.5 and a 10% increase in SUV for malignancy; the authors determined that the sensitivity and specificity of the tests were 80% and 94% (single) and 100% and 89% (dual), respectively (*36*). Pathophysiologically, the differences in levels of glucose-6-phosphatase and hexokinase within benign and malignant cells have been postulated as the reason for this effect (*37*). Although these studies appear promising, the use of dual-time-point imaging remains controversial. Further data are needed before widespread use can be recommended.

^{18}F-FDG PET is known to show little uptake in malignancies with low metabolic activity. Focal bronchioalveolar cell carcinoma has been shown to have less proliferative potential and a longer mean doubling time than NSCLC (*38,39*). Further investigation has shown that different subtypes of bronchioalveolar cell carcinoma exhibit different rates of metabolic activity. Focal or pure bronchioalveolar cell carcinoma appears as a peripheral nodule or localized ground-glass attenuation and may show false-negative results on ^{18}F-FDG PET (*40*). In contrast, the multifocal form appears as multiple nodules or ground-glass consolidation (*40*) and is detected at a relatively high sensitivity on ^{18}F-FDG PET (*41*). Carcinoid is another malignancy that grows slowly and has low mitotic activity (*42*). The sensitivity of ^{18}F-FDG PET for the detection of focal bronchioalveolar cell carcinoma and carcinoid tumor is lower than that for other cell types of lung cancer and has been reported to be as low as 50%.

Several groups have investigated the prognostic value of ^{18}F-FDG PET (*43–45*). In a study of 155 patients with NSCLC, median survival was compared with the standardized uptake ratio (analogous to the SUV) of the primary tumor (*43*). Median survival decreased with increasing mean SUV. SUVs of less than 10 and greater than 10 indicated median survival times of 24.6 and 11.4 mo, respectively (Fig. 5). Furthermore, a mean SUV of greater than 10 with a tumor larger than 3 cm indicated a median survival of 5.7 mo. A retrospective study of 100 patients demonstrated that the 2-y survival rates were 68% for patients with a maximum SUV of more than 9 and 96% for those with a maximum SUV of less than 9 (*45*).

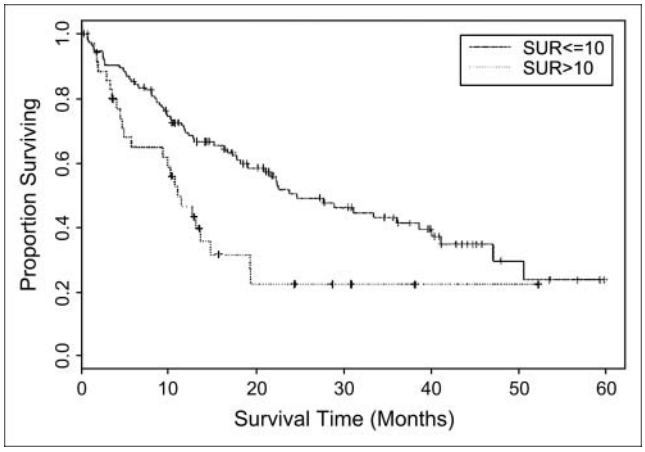

FIGURE 5. Survival among NSCLC patients stratified by standardized uptake ratio (SUR). (Reprinted with permission of (*43*).)

MULTIPLE PULMONARY NODULES

The evaluation of multiple pulmonary nodules can be limited by potential false-positive findings on ^{18}F-FDG PET. Increased ^{18}F-FDG activity has been demonstrated in instances of active granulomatous disease, such as tuberculosis, fungal disease, and sarcoidosis, as well as other inflammatory processes, such as rheumatoid nodules (*46,47*). CT in combination with ^{18}F-FDG PET aids in the evaluation of multiple pulmonary nodules. In addition to the shapes, borders, and densities of the nodules, the distribution of the nodules can provide important clues to their etiology. There are 3 different distribution patterns: perilymphatic, random, and centrilobular. Perilymphatic nodules are located along the pleural surfaces, interlobular septa, and peribronchovascular interstitium, particularly in the perihilar regions and centrilobular regions. Random nodules have a more even and symmetric, yet random, distribution within the lung fields bilaterally. Centrilobular nodules spare the pleural surfaces and are associated with small pulmonary artery branches. There are 2 subcategories of centrilobular pulmonary nodules, those associated with and those not associated with tree-in-bud opacities. A tree-in-bud opacity is a branching opacity that represents filling of the alveolar spaces. This process typically occurs from an inflammatory or infectious process rather than a malignant process. The remaining nodular distributions are more often associated with malignancy and include lymphangitic spread of cancer with a perilymphatic pattern, hematogenous metastasis with a random distribution, and bronchioalveolar cell cancer with centrilobular opacities.

STAGING OF LUNG CANCER

Before 1996, there were 2 mediastinal lymph node classification schemes. The 2 schemes were unified in 1996 by the American Joint Commission on Cancer and the Prognostic TNM Committee of the Union Internationale Contre le Cancer. As shown in Figure 6, thoracic lymph nodes can be organized into 4 groups: superior mediastinal, inferior mediastinal, aortic, and N1 nodes. These nodal groups can be divided further into anatomic lymph node regions or levels (Table 2) (*48*).

One of the uses of this lymph node classification is to identify the proper method for lymph node sampling. Different invasive procedures typically are used for lymph node sampling; these include mediastinoscopy, video-assisted thoracic surgery (VATS), endoscopic sonography, and thoracotomy (Table 3) (*49*). Mediastinoscopy is best used for the evaluation of level 2, 4, and 7 lymph node stations. VATS can be used for multiple stations, depending on the approach, and is commonly used for level 5, 6, and 10 stations. Endoscopic sonography with transbronchial needle aspiration can be used for level 4–9 stations. All nodal groups can be reached by thoracotomy and potentially by CT-guided percutaneous needle biopsy.

The location of the primary tumor determines the lymphatic pathway for spread to regional lymph nodes (*50*). A tumor in the right lung sends metastasis to hilar (10R) lymph nodes, which proceed to right paratracheal (4R and 2R) lymph nodes. Such a tumor rarely metastasizes to the contralateral side. A left upper-lobe cancer sends metastases to the aortopulmonary window (5) and left paratracheal nodes (4L). Left upper- and lower-lobelesions also may spread initially to left hilar (10L) lymph nodes. Involvement of prevascular (6) lymph nodes is almost invariably associated with paratracheal involvement. Tumors in the right middle lobe and bilateral lower lobes can metastasize early to subcarinal (7) nodes. Lower-lobe cancers also can send metastases to paraesophageal (8), pulmonary ligament (9), and subdiaphragmatic (14) lymph nodes.

CONVENTIONAL STAGING

The staging of malignancies with the TNM system was created to provide consistency in communication of the extent of disease, to provide a basis for the selection of therapy, and to help determine prognosis (*51*). The important decision in using this system is whether the disease is resectable. The T status classifies the features of the primary tumor. The N status classifies the presence or absence of regional lymph node involvement. The M status classifies the presence or absence of extrathoracic metastasis (Table 4).

The T status evaluates the extent of the primary tumor by size and invasiveness. The current system describes the size of the tumor and its relationship with the pleura, bronchovascular structures, and mediastinum. A T1 lesion is defined as a tumor that is 3 cm or smaller (in the greatest dimension), with lung or visceral pleura separating the lesion from the mediastinum, but that does not extend proximally to the lobar bronchus. A T2 lesion is larger than 3 cm, invades the visceral pleura, and extends proximally to the lobar bronchus but does not extend to within 2 cm of the carina. Extension of the primary tumor into the mediastinum precludes curative surgical resection (*52*). The preservation of mediastinal fat planes or intervening lung between the tumor and the mediastinum is a clear

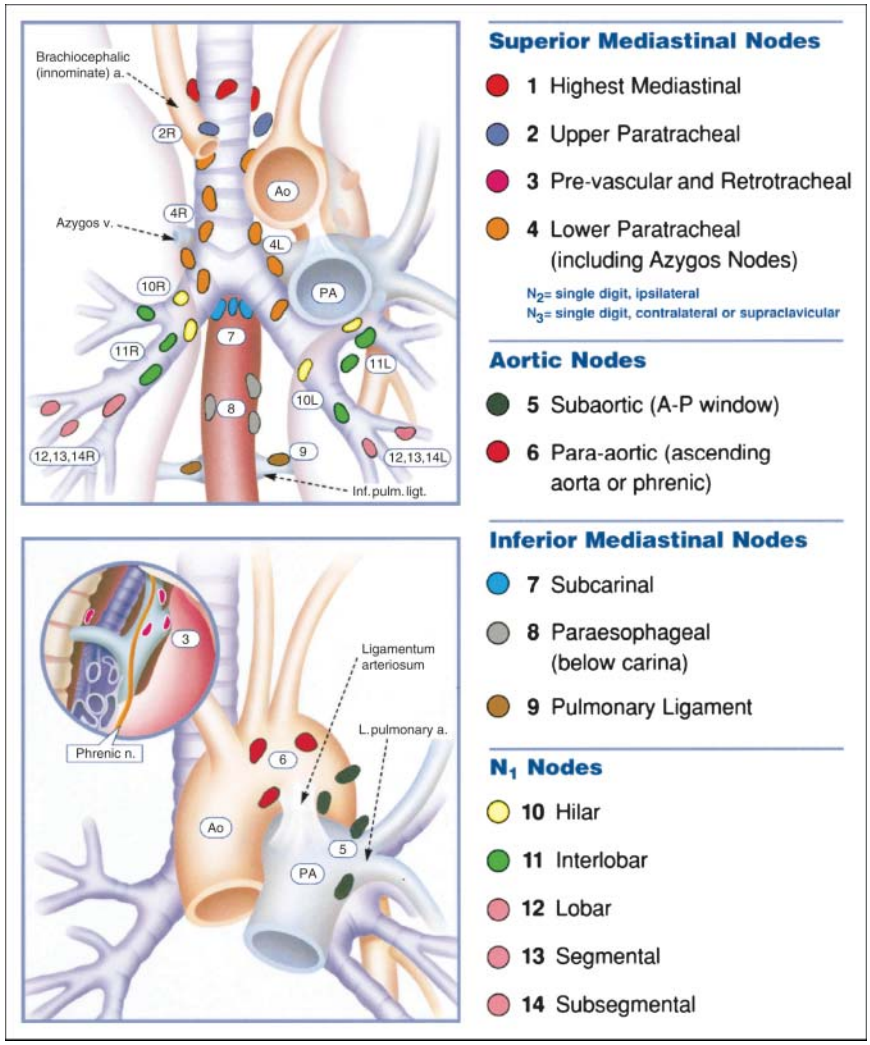

FIGURE 6. Thoracic lymph node stations. Subcategories include superior mediastinal nodes, aortic nodes, inferior mediastinal nodes, and N1 nodes (*64*). a. = artery; v. = vein; Inf. pulm. ligt. = inferior pulmonary ligament; Ao = aorta; PA = pulmonary artery; A-P = aortopulmonary; L. pulmonary a. = left pulmonary artery; Phrenic n. = phrenic nerve. (Reprinted with permission of (*64*).)

indication that there is no direct extension into the mediastinum. Extension into the chest wall, diaphragm, mediastinal pleura or pericardium, or main bronchus is defined as a T3 lesion. The presence of T3 lesions does not necessarily preclude curative resection. Invasion of the mediastinum, vertebrae, and vital structures, such as the great vessels, trachea, esophagus, or heart, is classified as a T4 lesion and does preclude curative resection.

Lymph node status (N status) is integral to determining the resectability of a tumor; it describes the presence or absence and extent of regional lymph node metastasis. Metastasis to lymph nodes in the ipsilateral peribronchial or hilar regions is classified as N1 disease, a classification that alters the stage and prognosis of disease. The presence of N1 lymph nodes, however, does not preclude curative resection and does not accurately predict mediastinal lymph node involvement. Metastatic involvement of ipsilateral mediastinal lymph nodes is defined as N2 disease and represents at least stage IIIA disease. The presence of contralateral mediastinal, hilar, scalene, or supraclavicular lymph node involvement is defined as N3 disease and increases the patient's clinical stage to stage IIIB or higher. At stage III, evaluation of the mediastinum for either direct extension to vital structures or contralateral mediastinal lymph node disease determines resectability.

The CT evaluation of mediastinal lymph nodes has extremely variable sensitivity and specificity, with false-negative results of 7%–39% and false-positive results of 20%–45% (*9*). Size criteria alone are not very reliable in the staging of mediastinal lymph nodes (*53,54*). Lymph nodes of greater than 1 cm in the short axis are considered abnormal by CT criteria (*55*). Fifteen percent of patients with clinical stage I disease may have micrometastases in normal-size lymph nodes (*56*). Other morphologic features of lymph nodes are unlikely to be helpful in differentiating benign disease from malignant disease (*57*). Fat within a lymph node hilum is believed to be a sign of benignity. Adenopathy detected by CT is useful in directing invasive sampling techniques. Mediastinoscopy traditionally has been used for tissue diagnosis of mediastinal lymph node metastasis; however, additional techniques, such as transbronchial, percutaneous, or videoscopic biopsy, may be used when appropriate.

TABLE 2
Lymph Node Map Definitions

Nodal station anatomic landmarks	Description
N2 nodes—all N2 nodes lie within mediastinal pleural envelope	
Highest mediastinal nodes	Nodes lying above horizontal line at upper rim of bracheocephalic (left innominate) vein, where it ascends to left, crossing in front of trachea at its midline
Upper paratracheal nodes	Nodes lying above horizontal line drawn tangential to upper margin of aortic arch and below inferior boundary of highest mediastinal nodes
Prevascular and retrotracheal nodes	Prevascular and retrotracheal nodes may be designated 3A and 3P; midline nodes are considered to be ipsilateral
Lower paratracheal nodes	Lower paratracheal nodes on right lie to right of midline of trachea between horizontal line drawn tangential to upper margin of aortic arch and line extending across right main bronchus at upper margin of upper-lobe bronchus and are contained within mediastinal pleural envelope; lower paratracheal nodes on left lie to left of midline of trachea between horizontal line drawn tangential to upper margin of aortic arch and line extending across left main bronchus at level of upper margin of left upper-lobe bronchus, medial to ligamentum arteriosum, and are contained within mediastinal pleural envelope
Subaortic (aortopulmonary window)	Subaortic nodes are lateral to ligamentum arteriosum, aorta, or left pulmonary artery and proximal to first branch of left pulmonary artery and lie within mediastinal pleural envelope
Paraaortic nodes (ascending aorta or phrenic)	Nodes lying anterior and lateral to ascending aorta and aortic arch or innominate artery, beneath line tangential to upper margin of aortic arch
Subcarinal nodes	Nodes lying caudad to carina of trachea but not associated with lower-lobe bronchi or arteries within lung
Paraesophageal nodes (below carina)	Nodes lying adjacent to wall of esophagus and to right or left of midline, excluding subcarinal nodes
Pulmonary ligament nodes	Nodes lying within pulmonary ligament, including those in posterior wall and lower part of inferior pulmonary vein
N1 nodes—all N1 nodes lie distal to mediastinal pleural reflection and within visceral pleura	
Hilar nodes	Proximal lobar nodes, distal to mediastinal pleural reflection, and nodes adjacent to bronchus intermedius on right; radiographically, hilar shadow may be created by enlargement of both hilar and interlobar nodes
Interlobar nodes	Nodes lying between lobar bronchi
Lobar nodes	Nodes adjacent to distal lobar bronchi
Segmental nodes	Nodes adjacent to segmental bronchi
Subsegmental nodes	Nodes around subsegmental bronchi

Reprinted with permission of (*64*).

Evaluation of distant metastasis (M status) also is a critical step in determining the resectability of a tumor. M status defines the presence or absence of tumor spread to distant lymph node or organ sites. The brain, central nervous system, bone, liver, and adrenal glands are common sites for distant metastases, and such extension is considered to represent M1 disease (*58*). Metastases to the contralateral lung also are considered distant metastases.

TABLE 3
Procedures Used to Sample Lymph Nodes, by Lymph Node Level

Lymph node level	Mediastinoscopy	Thoracotomy	Chamberlain/VATS	Esophageal sonography
2L, 2R	✓	✓		
4L, 4R	✓	✓		✓
5, 6		✓	✓	✓
7	✓	✓		✓
8, 9		✓		✓
10L, 10R		✓	✓	
11–14		✓		

Reprinted with permission of Society of Thoracic Surgeons (*49*).

TABLE 4
TNM Classification of Lung Cancer

Classification	Description
Primary tumor (T)	
TX	Primary tumor cannot be assessed; or tumor proven by presence of malignant cells in sputum or bronchial washes but not visualized by imaging or bronchoscopy
T0	No evidence of primary tumor
Tis	Carcinoma in situ
T1	Tumor 3 cm or less in greatest dimension, surrounded by lung or visceral pleura, without bronchoscopic evidence of invasion more proximal than lobar bronchus (i.e., not in main bronchus)
T2	Tumor with any of the following features of size or extent: more than 3 cm in greatest dimension; involves main bronchus, 2 cm or more distal to carina; invades visceral pleura; or associated with atelectasis or obstructive pneumonitis that extends to hilar region but does not involve entire lung
T3	Tumor of any size that directly invades any of following: chest wall (including superior sulcus tumors), diaphragm, mediastinal pleura, or parietal pericardium; tumor in main bronchus less than 2 cm distal to carina but without involvement of carina; or associated atelectasis or obstructive pneumonitis of entire lung
T4	Tumor of any size that invades any of following: mediastinum, heart, great vessels, trachea, esophagus, vertebral body, or carina; or tumor with malignant pleural or pericardial effusion or with satellite tumor nodule(s) within lobe of lung ipsilateral to lobe with primary tumor
Regional lymph nodes (N)	
NX	Regional lymph nodes cannot be assessed
N0	No regional lymph node metastasis
N1	Metastasis to ipsilateral peribronchial or ipsilateral hilar lymph nodes or both and involvement of intrapulmonary nodes by direct extension of primary tumor
N2	Metastasis to ipsilateral mediastinal or subcarinal lymph nodes
N3	Metastasis to contralateral mediastinal, contralateral hilar, ipsilateral or contralateral scalene, or supraclavicular lymph nodes
Distant metastasis (M)	
MX	Presence of distant metastasis cannot be assessed
M0	No distant metastasis
M1	Distant metastasis present

Reprinted with permission of (*51*).

The radiologic workup for metastatic disease often begins with clinical history, physical examination, and laboratory studies. The frequency of occult metastasis at the time of presentation may be as high as 30% in patients with adenocarcinoma or large cell carcinoma of the lung (*59*). Squamous cell carcinoma of the lung appears to have a lower frequency of occult metastasis (<15%) at presentation. Routine radiologic evaluation for occult metastases without clinical or laboratory findings is not clearly indicated (*60*). The adrenal glands and liver are the most common sites for occult extrathoracic metastases. The adrenal glands occasionally may be the only sites for metastasis; however, incidental benign adenomas occur with a similar frequency in patients with bronchogenic carcinomas. Three to 5% of the overall population has incidental nonfunctioning cortical adenomas, whereas approximately 10% of patients with bronchogenic cancer have an adrenal mass on CT (*61,62*). In the absence of other known extrathoracic metastases, adrenal masses usually are benign. The liver usually is never the only site for metastasis, unless the primary malignancy is an adenocarcinoma. CT and MRI traditionally have been used for the evaluation of distant metastasis. Unenhanced CT followed by MRI is reported as the most cost-effective morphologic evaluation of suggestive adrenal lesions (*63*). Adrenal lesions that measure less than 10 HU on unenhanced CT are considered benign. Adrenal lesions that do not have CT signs of benignity are followed up with MRI with opposed-phase imaging. ^{18}F-FDG PET is sensitive for the detection of adrenal metastases, but some benign adrenal adenomas may be abnormal on PET.

The International System for Staging Lung Cancer was developed in response to the need for a classification scheme to unify the variations in staging definitions and provide consistent meaning and interpretation for different stages. The value of this system in predicting prognosis relies on the identification of consistent and reproducible patient groups with similar outcomes. The International System for Staging Lung Cancer applies to all 4 major cell types of lung cancer: squamous cell, adenocarcinoma (including bronchioalveolar cell), large cell, and small cell. Multiple factors are directly related to the extent of disease at diagnosis; these include the proportion of patients achieving a complete response, the duration of the response, and recurrence after a complete response.

The TNM system is used to define 7 stages of disease (Table 5) (*51*). Stage IA includes small tumors of less than or equal to 3 cm, without invasion proximal to a lobar bronchus, and without metastasis. Stage IB includes larger tumors, tumors with invasion of the visceral pleura or main bronchus (>2 cm distal to the carina), or both, and tumors without metastasis. There is a significant difference in survival between IA disease and IB disease, with 5-y survival rates of 61% and 38%, respectively (*64*). Stage IIA includes T1 tumors with metastases to ipsilateral peribronchial lymph nodes, hilar lymph nodes, or both. These metastases are difficult to document radiographically. Stage IIB includes T2 lesions with metastases to ipsilateral peribronchial lymph nodes, hilar lymph nodes, or both and T3 tumors without metastasis. The 5-y survival rates for stage IIA and stage IIB are 37% and 24%, respectively (*64*). Stage IIIA includes T3 tumors with metastases to intrapulmonary lymph nodes, hilar lymph nodes, or both (N1). T1 through T3 tumors with ipsilateral mediastinal lymph node metastases (N2) also are included in IIIA disease. This stage includes limited invasion of the mediastinum or chest wall (T3). Such lesions have an improved outcome and are potentially resectable if vital structures in the mediastinum are not involved. Stage IIIB involves extensive extrapulmonary involvement, with invasion of the mediastinal structures, esophagus, trachea, carina, heart, major vessels, or vertebral bodies. An associated pleural effusion also is considered to represent stage IIIB disease. No distant metastatic disease is present. This stage of disease is virtually always nonresectable (*9*). The 5-y survival rates for stage IIIA and stage IIIB are 9%−13% and 5%, respectively (Fig. 7) (*64*). Stage IV includes any T status and N status with distant metastases. Non–lymph-node metastases in ipsilateral lobes not involved by the primary tumor also are considered stage IV disease. Stage IV disease is considered a contraindication to surgical resection (*9*). As expected, survival with stage IV disease is poor, with less than 1% survival at 5 y (*64*).

TABLE 5
International Staging System for NSCLC, Including Stage Groups and TNM Subsets

Stage	TNM subset
0	Carcinoma in situ
IA	T1 N0 M0
IB	T2 N0 M0
IIA	T1 N1 M0
IIB	T2 N1 M0, T3 N0 M0
IIIA	T3 N1 M0, T1 N2 M0, T2 N2 M0, T3 N2 M0
IIIB	T4 N0 M0, T4 N1 M0, T4 N2 M0, T1 N3 M0, T2 N3 M0, T3 N3 M0, T4 N3 M0
IV	Any T any N M1

Reprinted with permission of (*51*).

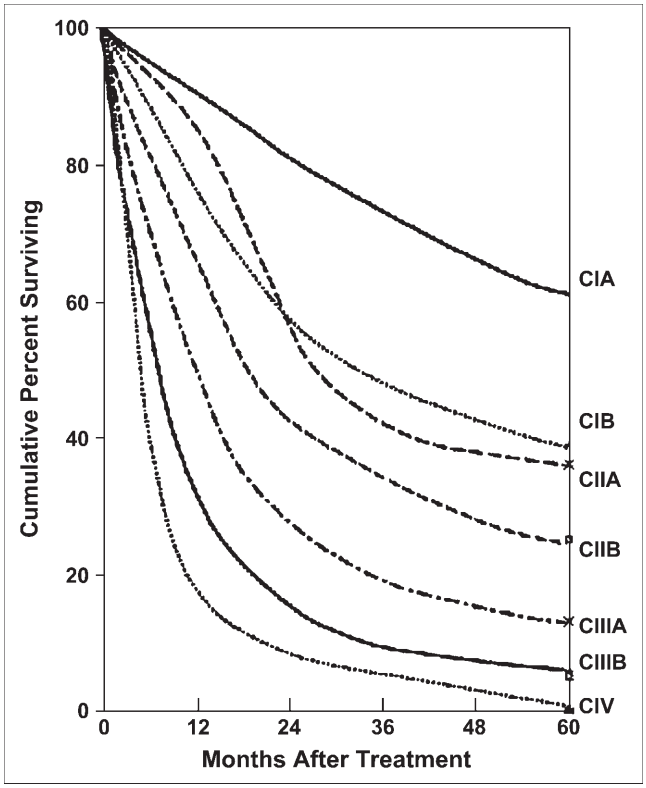

FIGURE 7. Patient survival in relation to stage of disease. c = clinical stage. (Reprinted with permission of (*51*).)

COMBINING CONVENTIONAL STAGING WITH METABOLIC IMAGING

As a measure of metabolic activity, ^{18}F-FDG PET adds a functional evaluation to the staging of lung cancer. The PET in Lung Cancer Staging trial attempted to determine the value of ^{18}F-FDG PET in lung cancer staging (*65*). The goal was to determine whether unnecessary surgery could be reduced. The researchers enrolled 188 patients in a randomized controlled trial comparing a conventional radiologic staging workup (CWU) to CWU and PET. The conclusions of the study were that the addition of PET to CWU prevented unnecessary surgery in 1 of 5 patients with suspected NSCLC. In addition, the staging of disease was increased for 27% of patients. The researchers believed that the negative predictive value of PET for mediastinal lymph node involvement was sufficiently high to avoid mediastinoscopy for noncentral tumors. Another prospective study of 102 patients went further to conclude that invasive procedures probably are not necessary in a patient with negative findings on PET for the mediastinum (*66*). In that study, the sensitivity and specificity of PET in detecting mediastinal lymph node metastasis were 91% and 86%, respectively.

The high negative predictive value of PET led some institutions to accept negative PET results without pathologic confirmation and to proceed to curative surgical resection. This management scheme has led to much controversy with regard to the role of PET in mediastinal staging. Although the PET in Lung Cancer Staging study demonstrated a clear

benefit of PET in predicting disease, the results may not be generalizable to other populations (*67*). The accuracy of clinical evaluation for distant metastasis in NSCLC has been investigated for each stage of the disease. These studies reported a 5% false-negative rate for the clinical evaluation of stage I and II diseases (*68–70*). The false-negative rate for stage III disease was reported to be 15%−20%. Without clinical evidence of distant metastatic disease, mediastinal involvement becomes a crucial issue in determining the stage of the disease. CT evaluation of the mediastinum has a false-negative rate of 15% overall; the false-negative rate increases to 20%−25% for central lung tumors (*71,72*). A meta-analysis of the diagnostic performance of PET versus CT for mediastinal staging was performed by Dwamena at al. (*73*). For 14 PET and 29 CT case series, they determined that PET was statistically superior to CT for mediastinal staging. With respect to CT, PET has been shown to have a higher negative predictive value, and combined PET/CT has an even higher negative predictive value (*49,74–76*).

The use of PET to exclude mediastinal metastasis remains controversial. From the data available, classification of disease as stage I on the basis of a clinical examination and negative results from CT and PET examinations appears sufficient to exclude mediastinal disease. Classification of stage II and III diseases is more controversial; the negative predictive value of PET decreases in relation to the size of the metastasis, the presence of centrally located primary disease or N1 nodes, and the avidity of the primary tumor for ^{18}F-FDG (*77,78*). Micrometastatic disease cannot be imaged effectively on PET because of the spatial resolution of the imaging system (*79,80*). Takamochi et al. found that the diameters of false-negative lesions ranged from 1 to 7.5 mm (*80*). In addition, the presence of hypermetabolic central tumors or hilar lymph nodes can decrease the detectability of mediastinal lymph nodes and thus the negative predictive value of mediastinal PET (*78*). Finally, the metabolic activity of low-grade malignancies cannot be expected to be any greater than that of the primary tumor (*77*). Mediastinal activity is a source of potential error attributable to random inhomogeneity and misregistration from respiratory, cardiac, and body motions. For stage II and III diseases, the incidence of false-negative results is still greater with PET than with mediastinoscopy. In a comparative study, the false-negative rates of mediastinoscopy and PET were 3% and 11.7%, respectively (*81*). Mediastinoscopy likely will remain part of the standard protocol for mediastinal staging for stage II and III diseases. The clinical importance of differentiating stage IIIA and IIIB diseases, with regard to denying curative resection, is a significant factor in the continued use of mediastinoscopy. Several studies have demonstrated the potential of PET to alter patient management (*82–84*). Hicks et al. found that PET caused a major management change in 40 of 63 patients (63%) who had previously undergone potential curative surgery for NSCLC (*82*). Seltzer et al. demonstrated that PET changed the staging of lung cancer in 44% of cases (*83*). The use of PET in stage IV disease is less of an issue for mediastinal staging, as the patient's N status is no longer relevant. The use of PET in stage IV disease will be discussed further with regard to identifying and monitoring distant metastasis.

Because ^{18}F-FDG describes metabolic activity, it cannot distinguish malignancy from inflammation or infection. ^{18}F-FDG uptake is demonstrated in sites of active acute inflammation because of increased glucose uptake by activated macrophages and inflammatory cells (*85*). Multiple studies have demonstrated a positive predictive value for PET of 74%−93% for evaluation of the mediastinum (*66,86*). A study comparing PET and mediastinoscopy evaluations of 202 patients showed a positive predictive value for PET of 44.6% (*81*). The high rate of false-positive results demonstrates the necessity for mediastinoscopy in the staging of PET-positive mediastinal lymph nodes (*80*,*87*). The added benefits of PET in this setting include the ability to direct mediastinal lymph node biopsy and to aid in selecting additional invasive methods for lymph nodes inaccessible to mediastinoscopy (Table 3).

STAGING OF SMALL CELL LUNG CANCER (SCLC)

SCLC represents approximately 18%−25% of all cases of lung cancer (*88,89*). SCLC is a neuroendocrine tumor that has an aggressive growth pattern, that commonly displays early widespread metastases, and that has a rapid tumor doubling time (*90*). Consequently, patients often present with bulky hilar and mediastinal lymph node metastases (*91*). The tumors usually are located centrally (*89,92*), often with encasement of mediastinal structures and tracheobronchial compression (*91,93*). The primary tumor may be small or undetectable by radiographic methods, whereas early extrathoracic metastases are common and can present before clinical symptoms (*94,95*). Unlike the situation for NSCLC, there is a 2-stage classification scheme proposed by the Veterans Administration Lung Cancer Study Group. Patients with SCLC are classified as having either limited or extensive disease (*96*). Limited disease refers to tumor that is confined to the thorax. Extensive disease includes distant metastases, including those to the contralateral lung. Whether ^{18}F-FDG PET has a role in the staging of SCLC is controversial. Detterbeck et al. stated that the clinical presentation and radiographic appearance are sufficiently characteristic of the disease to eliminate the need for further confirmation (*97*). A few studies have been performed to compare the staging of SCLC by conventional radiography with that by ^{18}F-FDG PET. PET changed patient management in 8.3%−29% of these cases (*98–101*). Patients with limited disease were given chemoradiation, whereas patients with extensive disease were given chemotherapy alone. The available studies show a possible role for ^{18}F-FDG PET in the staging of SCLC; however, further study is necessary to evaluate the clinical necessity.

COST-EFFECTIVENESS OF STAGING BY PET

The cost-effectiveness of PET for the staging of NSCLC has been extensively studied in multiple health care systems. Cost-effectiveness is analyzed with respect to the cost of patient care and life expectancy. The incremental cost-effectiveness ratio quantifies the difference in cost for different therapeutic strategies versus the difference in life expectancy (*102*). A study comparing 5 different clinical strategies was performed with Medicare reimbursements in the United States as the basis for the cost analysis. Conventional CT staging followed by biopsy and surgical versus nonsurgical therapy was compared with 4 strategies integrating PET. Three strategies used confirmatory biopsy before diverting patients from curative resection. The final strategy eliminated confirmatory biopsy and proceeded to surgical or nonsurgical therapy. That study demonstrated that the most cost-effective strategy involved the use of PET for CT evaluations with negative results followed by confirmatory biopsy. The strategy involving the elimination of confirmatory biopsy after CT and PET evaluations with positive results had the lowest cost but also the lowest life expectancy (*103*). A direct comparison of the cost-effectiveness of PET for demonstrating additional or unanticipated results using PET with confirmatory mediastinoscopy and PET with selective mediastinoscopy demonstrated a savings in both instances. Selective mediastinoscopy showed approximately double the cost savings per patient ($2,267 vs. $1,154) but missed 1.7% of patients who might be cured (*104*). A comparison of cost-effectiveness in other health care systems is more difficult because of the use of different therapeutic strategies. A study of the French health care system involved a significant difference in staging strategies (*105*). The therapeutic strategies in that study did not mandate confirmatory biopsy before surgical or nonsurgical therapy. That study determined that the most cost-effective strategy involved the use of PET after a CT examination with negative or positive results. The PET results then were used to make decisions regarding biopsy, surgery, or chemotherapy. Similar findings were demonstrated in studies of the Italian (*29*), Canadian (*106*), and German (*107*) health care systems. Irrespective of the use of mediastinoscopy, PET for the evaluation of mediastinal disease in NSCLC has been shown to be cost-effective in several health care models.

DETECTION OF DISTANT METASTASIS

The presence of distant metastasis is classified as stage IV disease, which precludes a patient from the possibility of curative surgical resection. The patient therefore is prescribed palliative therapy. An inherent advantage of PET is the use of whole-body scanning, which facilitates the survey of a much larger area than is possible with commonly used radiographic methods (Fig. 8). Distant metastases commonly involve the adrenal glands, bones, liver, and brain (*108*). Multiple studies have demonstrated the ability of ^{18}F-FDG PET to detect distant metastasis of lung cancer with greater specificity than can conventional imaging, including CT (*109*). The mean frequency of extrathoracic metastases in these studies was 13%. In 18% of the cases, the PET results altered management. As expected, the frequency of distant metastases was shown to increase with higher stages: 7.5% in stage I, 18% in stage II, and 24% in stage III (*110*).

As discussed earlier, the adrenal glands and liver are the most common sites of extrathoracic metastases in lung cancer. At the time of presentation, up to 10% of patients will have an adrenal mass. Approximately two thirds of these masses will be benign (*111,112*). In a study of 27 patients with 33 adrenal masses, the ability of PET to differentiate benign from malignant adrenal masses was investigated (*113*). The sensitivity of PET for detecting adrenal metastasis was 100%, and the specificity was 80%. A subsequent study of adrenal lesions demonstrated a sensitivity of 100%, a specificity of 94%, and an accuracy of 96% for detecting metastasis (*114*). The evaluation of liver metastasis by PET is less well studied. Liver metastases are rarely the only demonstrable site of metastatic disease (*9*).

In a study of 110 patients with NSCLC, ^{18}F-FDG PET was compared with methylene diphosphonate bone scanning for the evaluation of bone metastases (*115*). ^{18}F-FDG PET had a higher specificity for detecting bone metastases (98% vs. 61%). Some additional studies demonstrated a higher specificity (*116,117*), and some demonstrated a higher accuracy (*115,118,119*). Marom et al. (*120*) found that, compared with bone scintigraphy, ^{18}F-FDG PET had a higher sensitivity but an equivalent specificity for 90 patients who underwent both studies. Fogelman et al. (*121*) reviewed the literature on this topic and concluded that, with regard to lung cancer, ^{18}F-FDG PET had a sensitivity similar to that of bone scintigraphy but a specificity higher than that of bone scintigraphy. The practical advantage of ^{18}F-FDG PET over bone scintigraphy remains controversial. Mechanistically, there are different patterns of uptake related to the morphology of the lesion: lytic, sclerotic, or mixed (*121*). As demonstrated in a study of breast cancer patients with bone metastases, ^{18}F-FDG PET appears to have the advantage of detecting osteolytic lesions, whereas bone scintigraphy has the advantage of detecting osteoblastic lesions (*122*).

The detection of brain metastasis by PET also has been evaluated. In a study of 1,026 patients with multiple different malignancies, unsuspected cerebral or skull metastases were detected in only 0.4% of the patients (*123*). PET is less effective than CT or MRI for the detection of cerebral metastasis.

RESTAGING

The benefit of determining a metabolic response to therapy over a morphologic response has led to the investigation of PET for the restaging of NSCLC. The criteria for conventional restaging were determined by the World Health Organization and later modified by the National

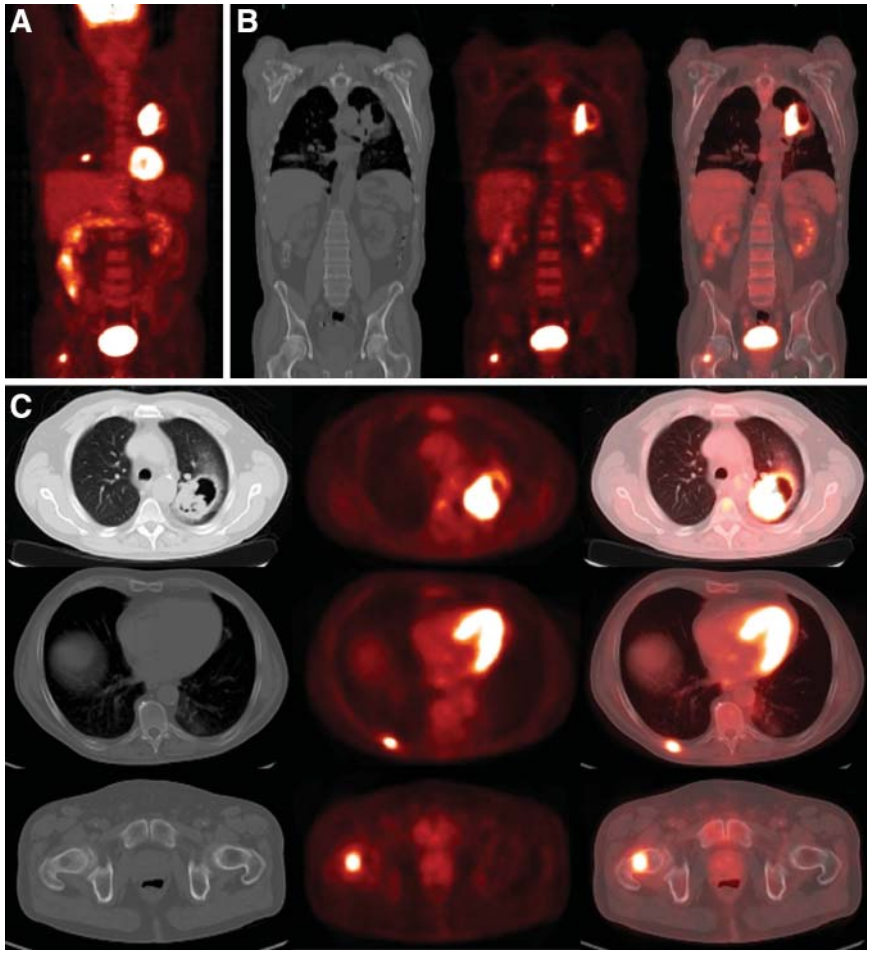

FIGURE 8. Lung cancer with osseous metastases. Hypermetabolic cavitary lung mass is seen in left upper lobe (A–C). Maximum-intensity-projection image (A) demonstrates additional lesions in contralateral thorax and hip. Additional focus of hypermetabolism is seen in right femoral neck (A–C) and corresponds to subtle lytic lesion on CT. Axial images (C) show hypermetabolism in right posterior 8th rib without osseous changes on CT.

Cancer Institute and the European Association for Research and Treatment of Cancer. Tumor response is defined as a therapy-induced reduction of the largest dimension of the tumor by 30% (*124*). Complete and partial responses are determined by the amount of tumor size reduction. Measuring and evaluating the morphologic response to therapy is less than ideal. A morphologic response to therapy usually occurs over several weeks to months. During the interim, patients with nonresponding tumors are treated without benefit. In addition, morphologic evaluation can be inaccurate because of peritumoral scar tissue formation and edema, which can mask tumor regression (*125*).

PET has been investigated in 3 different scenarios: restaging after neoadjuvant therapy, early assessment of response to therapy, and restaging after completion of therapy. In the first scenario, PET could be used after induction chemotherapy or chemoradiation to evaluate for tumor resectability. Few studies have been performed to investigate the reliability of PET in assessing mediastinal "downstaging." From the studies that are available, it appears that there is much variability in the results (*97*). Studies evaluating for a complete pathologic response appear to have high false-positive and false-negative rates (*126–129*). The second scenario was investigated in a study of 57 patients who were evaluated by PET 1 wk before and 3 wk after the first cycle of chemotherapy (*130*). It was found that a reduction in metabolic activity correlated closely with the final outcome of the therapy. An early metabolic response predicted better survival, and a poor response predicted disease progression within the first 3 cycles of chemotherapy. The impact of this evaluation on the morbidity and cost of nonresponding tumors suggests much merit in this strategy. The third scenario is the most commonly performed scenario for restaging. Multiple studies have demonstrated a high specificity for the characterization of viable tumor and scar tissue after therapy (*109*). Furthermore, Patz et al. have shown that ^{18}F-FDG PET has prognostic value and correlates strongly with rates of survival of patients with treated lung cancer; patients with positive ^{18}F-FDG PET results have a significantly worse prognosis than patients with negative results (*131*). Hicks et al. demonstrated a significant impact of PET on further management, with major changes being made in 63% of studied cases (*82*).

RADIATION THERAPY PLANNING

Radiation therapy currently involves CT-based planning to provide radiation selectively to a tumor. In lung cancer, the chest is a critical area for treatment planning because of the vital structures in close proximity to treatment ports.

Limiting radiation strictly to tumor tissue may be nearly impossible, and nontarget tissues are inevitably affected. PET has been investigated for refining treatment volumes for the purpose of limiting them to allow an increase in dose to target tissues and a reduction in toxicity to nontarget tissues. In a retrospective study of 34 patients, Nestle et al. determined that the use of PET would have led to a substantial reduction in the size of radiation portals (*132*). Multiple studies have demonstrated significant changes in target volumes after planning with PET (*133–137*).

PLEURAL DISEASE

^{18}F-FDG PET has been used to evaluate pleural fluid and pleural masses for evidence of malignancy. Erasmus et al. evaluated 25 patients with suspected malignant pleural effusions (*138*). They reported the sensitivity, specificity, and positive predictive value to be 95%, 67%, and 95%, respectively. With a high positive predictive value, ^{18}F-FDG PET is likely to improve staging in patients with NSCLC. A later study of 92 patients compared the utility of ^{18}F-FDG PET with that of CT in the differentiation of benign from malignant pleural effusions (*139*). A total of 71% of pleural effusions seen on CT were indeterminate for malignancy. With ^{18}F-FDG PET, the sensitivity, specificity, and positive predictive value were 100%, 71%, and 63%, respectively. The difference in positive predictive values may be attributable to the larger number of benign pleural effusions included in the more recent study. Despite some differences in results, ^{18}F-FDG PET was found to be useful for the evaluation of suspected malignant pleural effusions (Fig. 9). ^{18}F-FDG PET likely will provide information complementary to that obtained with other methods, because the results of fluid cytologic analysis have been reported to be positive for only 66% of malignant pleural effusions from NSCLC (*140*).

CT is commonly used to diagnose, stage, and monitor treatment response for malignant pleural mesothelioma (MPM). The CT findings associated with mesothelioma include a unilateral pleural effusion, nodular pleural thickening, interlobar fissure thickening, and tumor invasion of the chest wall, mediastinum, and diaphragm (*141*). In a study of 20 patients, CT was shown to have limitations in the evaluation of chest wall, transdiaphragmatic, and peritoneal involvement, as well as mediastinal involvement (*142*). Several studies have demonstrated a sufficient elevation in ^{18}F-FDG accumulation within malignant pleural mesotheliomas to distinguish benign from malignant pleural disease (*143–146*). In a study of 15 patients with MPM, the impact of PET on staging was evaluated (*147*). For 13% of patients, the staging of disease was increased, whereas for 27% of patients, the staging of disease was decreased, leading to the conclusion that ^{18}F-FDG PET played a worthwhile role in staging. Erasmus et al. evaluated the role of PET/CT in patients who had MPM and who were being evaluated for surgery (extrapleural pneumonectomy) (*148*). That study of 29 patients determined that PET/CT can improve the accuracy of M staging, resulting in a more appropriate selection of surgical candidates. Erasmus et al. found limitations of PET in T staging and N staging. Further investigation is necessary to determine the specific uses of PET in the staging of MPM. In addition to staging, ^{18}F-FDG PET may be useful in the prognosis of patients with MPM. Flores evaluated the risk of mortality from MPM in 65 patients and determined that patients with tumors with an SUV of greater than 4 had a 3.3-fold greater risk of death than did patients with tumors with a lower SUV (*149*).

EVALUATING PET SCANS

In the examination of thoracic PET studies, it is helpful to review regions of physiologic ^{18}F-FDG uptake, normal variants, and nonmalignant causes of ^{18}F-FDG uptake. Areas directly relevant to thoracic PET include the neck, thorax, and upper abdomen. Table 6 describes potential false-positive findings on ^{18}F-FDG PET. Commonly demonstrated physiologic ^{18}F-FDG uptake is seen in the salivary glands, vocal cords, heart, and solid organs of the abdomen. ^{18}F-FDG uptake has been demonstrated within the walls of the aorta and great vessels. This finding correlates with the patient's age and hypercholesterolemia and may represent areas of atherosclerosis (*150–152*). The esophagus may show physiologic ^{18}F-FDG uptake or uptake within areas of esophagitis, Barrett's esophagus, and gastroesophageal reflux (*153*). The thymus typically shows physiologic ^{18}F-FDG uptake in children less than 13 y old. Uptake within the thymus also can be seen after chemotherapy (*154*). Thymic hyperplasia is thought to be due to chemotherapeutic drugs causing increased uptake

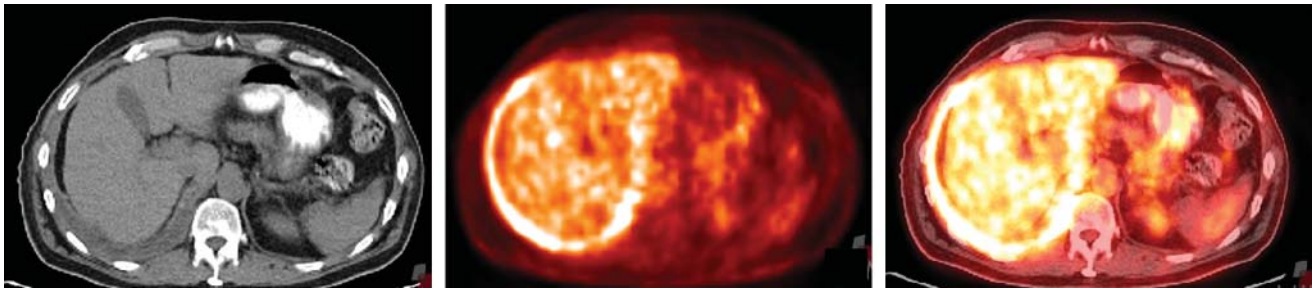

FIGURE 9. Malignant pleural effusion in right hemithorax. Hypermetabolism is associated with this effusion, consistent with malignant pleural effusion.

TABLE 6
Possible Causes of False-Positive Findings in ^{18}F-FDG PET Studies in Chest

Category, location, and finding	Cause
Infection or Inflammation	
Lung	
Fungal	Aspergillosis; cryptococcosis; blastomycosis; coccidioidomycosis
Mycobacterial	Active tuberculosis; atypical mycobacteriosis
Bacterial	Pneumonia; abscess; nocardiosis
Granuloma	Granuloma; necrotizing granuloma; sarcoidosis; Wegener granulomatosis; plasma cell granuloma; histoplasma granuloma; rheumatoid arthritis–associated lung disease
Interstitial fibrosis	Radiation pneumonitis; fibrosing alveolitis
Occupational	Inflammatory anthracosilicosis
Allergic	Airway inflammation with asthma
Nonspecific	Inflammation; acute inflammation with bronchiectasis and atelectasis; reactive mesothelial cell; tumor necrosis; histiocytic infiltrate; inflammatory pseudotumor; fibrous histiocytic infiltrate; aspiration pneumonia with barium; aspiration pneumonia with salivary and tracheal secretions; organizing pneumonia
Pleura	Pleural effusion; empyema
Mediastinum (esophagus)	Esophagitis
Benign tumor	
Mediastinum (lymph node)	Chronic nonspecific lymphadenitis; cryptococcosis; tuberculosis; anthracosilicosis; active granuloma
Pleura	Fibrous mesothelioma
Nerve root	Schwannoma; aggressive neurofibroma
Bone	Chondrohamartoma; enchondroma
Physiologic uptake	
Muscle	Hypermetabolism after physical activity
Thymus	Normal until puberty; hyperplasia after chemotherapy
Bone marrow	Hyperplasia after chemotherapy
Brown fat	Nonshivering thermoregulation
Iatrogenic	
Skin and soft tissue	Open lung biopsy; irradiation
Trachea	Tracheostomy tube

Reprinted with permission of Edizioni Minerva Medica (*109*).

in patients up to 30 y old (*155*). Physiologic muscular uptake can occur from muscular contraction during tracer uptake. Commonly observed muscular uptake occurs in the trapezius, scalenius, genioglossus, sternocleidomastoid, paraspinal, and diaphragm muscles. Hickeson et al. showed that patients with chronic obstructive pulmonary disease may be predisposed to having thoracic and abdominal muscular uptake (*156*). Diffuse muscular uptake can be caused iatrogenically. The administration of insulin before the injection of ^{18}F-FDG causes diffusely increased skeletal muscle uptake (*157*). Brown fat is a

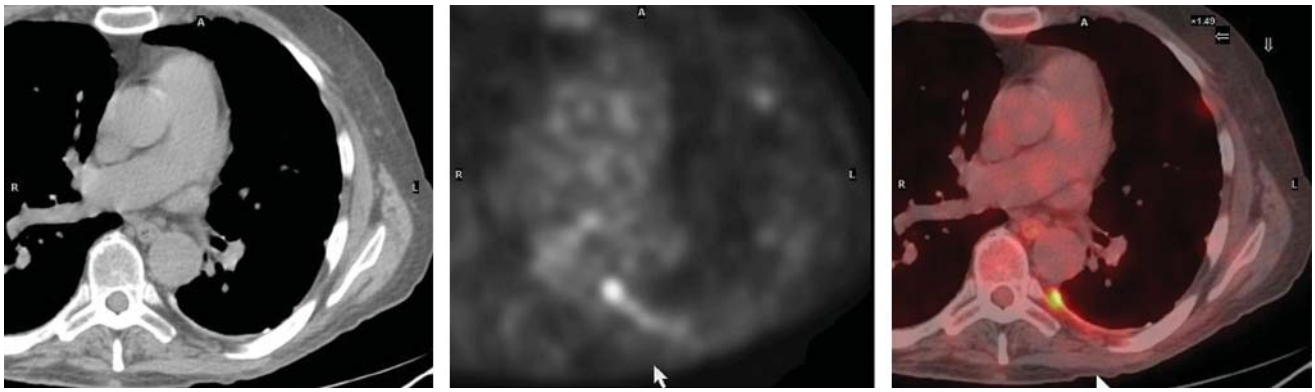

FIGURE 10. Pleurodesis. CT demonstrates left posterior pleural thickening. Hypermetabolism is associated with this area of pleural thickening. Additional sites of pleural hypermetabolism were seen throughout left pleural space on whole-body images. Patient had had pleurodesis in past, consistent with current findings.

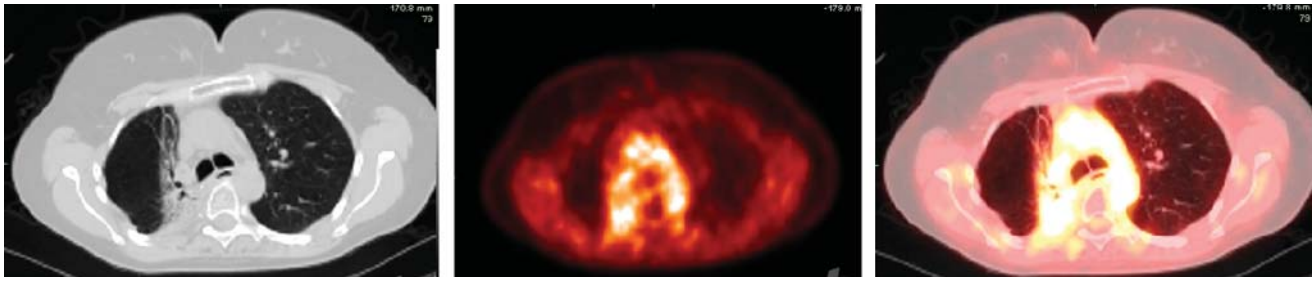

FIGURE 11. Radiation pneumonitis. Heterogeneous opacities demonstrated in a ''geometric configuration'' (straight edges) within medial right lung correspond to radiation therapy portal. Associated hypermetabolism is seen.

well-described site of physiologic ^{18}F-FDG uptake commonly located in the cervical, axillary, paravertebral, mediastinal, and abdominal regions. The distribution usually is bilateral and symmetric but may be asymmetric and focal (*158*). Joints and bone may show ^{18}F-FDG uptake from inflammatory or arthritic processes (*159*). Abnormal bone uptake also can be shown from benign and malignant bone tumors, osteomyelitis, acute fractures, Paget's disease, bone infarcts, pseudofractures, and poststernotomy wounds (*160*). Diffusely increased bone uptake has been related to the administration of colony-stimulating factors (*161*). Multiple iatrogenic causes of ^{18}F-FDG uptake have been reported; these include axillary nodal uptake from the infiltration of an ^{18}F-FDG dose and pericatheter uptake from tracheostomies, central venous catheters, chest tubes, gastrostomy tubes, and other drainage tubes. Various interventions can produce uptake in healing wounds; these include sternotomy, needle biopsies, mediastinoscopy, thoracotomy, and talc pleurodesis (Fig. 10). Radiation has been shown to produce pneumonitis (Fig. 11) as well as esophagitis. Asymmetric vocal cord uptake may be caused by paralysis of one of the vocal cords by compression of the recurrent laryngeal nerve. One of the treatments for vocal cord paralysis, which involves Teflon (DuPont) injection, also may cause focal ^{18}F-FDG uptake (*162*).

TUMOR EVALUATION

A qualitative comparison of tumor uptake may be sufficient to determine whether viable tumor is present after therapy. A quantitative analysis may be necessary during treatment to predict subsequent tumor response (*125*). Table 7 lists the factors involved in the tumor uptake of ^{18}F-FDG. Multiple other factors, aside from tumor metabolism, affect ^{18}F-FDG uptake (*163,164*). The partial-volume effect resulting from the limited spatial resolution of PET causes an underestimation of the true activity present. It has been shown that only 60% of maximal activity is measured in a lesion at 1.5 times the spatial resolution of the PET camera. Only at 4 times the spatial resolution does the difference between measured peak activity and true activity become less than 5% (*165*). The processing or "smoothing" of images with a gaussian filter also decreases image resolution and apparent ^{18}F-FDG uptake.

Tumoral uptake of ^{18}F-FDG increases with increasing time between injection and scanning. Glucose levels cause changes in ^{18}F-FDG uptake because of direct competition with glucose for accumulation. Finally, ^{18}F-FDG is not identical to glucose. ^{18}F-FDG and glucose differ in rates of phosphorylation, transport, and volume of distribution. To quantify the rate of metabolism of glucose, a conversion factor is used, but this constant also varies with the type of tissue examined. Table 8 summarizes the common sources of SUV measurement error.

FUTURE DIRECTIONS

As alluded to previously, there are multiple avenues of investigation that could be used to improve the ability of PET to diagnose and stage malignancies. One avenue that has received attention is improving the coregistration of lung tumors on PET/CT. In a study of 8 patients with 13 thoracic tumors, the researchers compared the SUVs of the tumors

TABLE 7
Factors That Can Affect Measured ^{18}F-FDG Uptake Within Tumors (*125*)

Factor	Effect
Lesion size	Marked underestimation of tracer uptake in lesions with diameter of <2 times resolution of PET scanner
Tumor heterogeneity	Underestimation of tracer uptake (e.g., lesions with necrotic center and relatively thin rim of viable tumor tissue)
Reconstruction parameters	Decrease in tracer uptake with ''smoother'' reconstruction parameters (filters, no. of iterations)
Region-of-interest definition	Lower mean uptake for larger regions of interest; larger random errors for small regions of interest
Blood glucose levels	Lower uptake with increasing blood glucose levels
Time after tracer injection	Increase in ^{18}F-FDG uptake with increasing time after injection

TABLE 8
Common Sources of Errors in Measurement of SUV (*125*)

Error	Effect on tumor SUV
Paravenous ^{18}F-FDG injection, residual activity in syringe	Incorrectly low SUV because area under plasma time–activity curve is smaller
No decay correction of injected activity	Incorrectly low SUV
Incorrect cross-calibration of scanner and dose calibrator	Incorrectly low or high SUV, depending on error of calibration factor
Variable uptake period (time between injection and imaging)	Higher SUV with longer uptake period

determined by attenuation correction with conventional helical CT (HCT) versus averaged CT with respiratory gating (ACT) (*166*). A difference of greater than 50% in the maximum SUV was demonstrated between the HCT and the ACT data for 4 of the 13 tumors. A significant reduction in diaphragmatic misregistration also was found with the ACT images. The researchers concluded that ACT provides a more accurate attenuation map for SUV quantitation. Further investigation is warranted, but it appears that respiratory gating provides potential improvements in quantitative and qualitative evaluations of thoracic malignancies.

A second avenue of investigation involves image processing and display formats for enhanced reader detectability. In a study of 15 patients with 21 intraluminal tumors, the researchers compared the detectability and localization of these lesions by conventional PET/CT and PET/CT virtual bronchoscopy and colonography (*167*). The data demonstrated 100% detection of lesions on virtual 3-dimensional images versus axial images and demonstrated subjective improvements. This initial work shows the potential improvement that can be obtained in detectability and localization by use of 3-dimensional display modes with fused PET/CT images.

A third avenue of investigation is the determination of the potential benefit of other PET radiotracers compared with the benefit of ^{18}F-FDG. Other radiotracers, such as ^{18}F-fluorothymidine (^{18}F-FLT) and ^{18}F-fluorocholine (^{18}F-FCH), are being investigated for use in lung cancer. Buck et al. (*168*) compared the diagnosis and staging of lung cancer with ^{18}F-FDG and ^{18}F-FLT in 43 patients. They concluded that ^{18}F-FLT had a higher specificity for malignant lung tumors; however, ^{18}F-FLT was less accurate for N staging and M staging. Cobben et al. (*169*) compared ^{18}F-FLT and ^{18}F-FDG in 17 patients with NSCLC. ^{18}F-FLT demonstrated a significantly lower maximum SUV in NSCLC than did ^{18}F-FDG. They concluded that ^{18}F-FLT was not useful in the staging or restaging of NSCLC. Similarly, ^{18}F-FCH has been compared with ^{18}F-FDG as a potentially useful tumor imaging agent. Tian et al. (*170*) compared ^{18}F-FCH and ^{18}F-FDG in 38 patients with various tumors, including 6 patients with lung cancer. They found similar radiotracer uptake in the known tumors, without clear improvement with ^{18}F-FCH over ^{18}F-FDG. Neither ^{18}F-FLT nor ^{18}F-FCH has shown clear improvement over ^{18}F-FDG at this time; therefore, they have no role at present.

REFERENCES

1. Spiro SG, Silvestri GA. One hundred years of lung cancer. *Am J Respir Crit Care Med.* 2005;172:523–529.
2. Adler I. *Malignant Growth of the Lung and Bronchi.* New York, NY: Longman, Green and Co.; 1912.
3. Doll R, Hill AB. Smoking and carcinoma of the lung: a preliminary report. *Br Med J.* 1950;2:739–748.
4. U.S. Public Health Service. *Surgeon General's Advisory Committee on Smoking and Health.* Washington, DC: U.S. Public Health Service; 1964. Publication 1103.
5. Mack MJ, Hazelrigg SR, Landreneau RJ, Acuff TE. Thoracoscopy for the diagnosis of the indeterminate pulmonary nodule. *Ann Thorac Surg.* 1993; 56:825–832.
6. Hoekstra CJ, Stroobants SG, Smit EF, et al. Prognostic relevance of response evaluation using [^{18}F]-2-fluoro-2-deoxy-D-glucose positron emission tomography in patients with locally advanced non-small-cell lung cancer. *J Clin Oncol.* 2005;23:8362–8370.
7. Hazelton TR, Coppage L. Imaging for lung cancer restaging. *Semin Roentgenol.* 2005;40:182–192.
8. Mavi A, Lakhani P, Zhuang H, Gupta NC, Alavi A. Fluorodeoxyglucose-PET in characterizing solitary pulmonary nodules, assessing pleural diseases, and the initial staging, restaging, therapy planning, and monitoring response of lung cancer. *Radiol Clin North Am.* 2005;43:1–21.
9. Lee JKT, Sagel SS, Stanley RJ, Heiken JP. *Computed Body Tomography with MRI Correlation.* 3rd ed. Philadelphia, PA: Lippincott Williams & Wilkins; 1998.
10. Proto AV, Thomas SR. Pulmonary nodules studied by computed tomography. *Radiology.* 1985;156:149–153.
11. Siegelman SS, Khouri N, Leo FP, Fishman EK, Braverman RM, Zerhouni EA. Solitary pulmonary nodules: CT assessment. *Radiology.* 1986;160:307–312.
12. Swensen SJ, Brown LR, Colby TV, Weaver AL. Pulmonary nodules: CT evaluation of enhancement with iodinated contrast material. *Radiology.* 1995;194:393–398.
13. Swensen SJ, Brown LR, Colby TV, Weaver AL, Midthun DE. Lung nodule enhancement at CT: prospective findings. *Radiology.* 1996;201:447–455.
14. Henschke CI, Yankelevitz DF, Mirtcheva R, McGuinness G, McCauley D, Miettinen OS. CT screening for lung cancer: frequency and significance of part solid and nonsolid nodules. *AJR.* 2002;178:1053–1057.
15. Nomori H, Watanabe K, Ohtsuka T, Naruke T, Suemasu K, Uno K. Evaluation of F-18 fluorodeoxyglucose (FDG) PET scanning for pulmonary nodules less than 3 cm in diameter, with special reference to the CT images. *Lung Cancer.* 2004;45:19–27.
16. Erasmus JJ, McAdams HP, Connolly JE. Solitary pulmonary nodules: part II. Evaluation of the indeterminate nodule. *RadioGraphics.* 2000;20:59–66.
17. Lillington GA, Caskey CI. Evaluation and management of solitary pulmonary nodules. *Clin Chest Med.* 1993;14:111–119.
18. Yankelevitz DF, Henschke CI. Does 2 year stability imply that pulmonary nodules are benign? *AJR.* 1997;168:325–328.
19. Gurney JW. Determining the likelihood of malignancy in solitary pulmonary nodules with Bayesian analysis. *Radiology.* 1993;186:405–413.
20. Black WC, Armstrong P. Communicating the significance of radiologic test results: the likelihood ratio. *AJR.* 1986;147:1313–1318.
21. Bernard A. Resection of pulmonary nodules using video assisted thoracic surgery. *Ann Thorac Surg.* 1996;61:202–204.
22. Gupta NC, Maloof J, Gunel E. Probability of malignancy in solitary pulmonary nodules using fluorine-18-FDG and PET. *J Nucl Med.* 1996;37:943–948.
23. Dewan NA, Shehan CJ, Reeb SD, Gobar LS, Scott WJ, Ryschon K. Likelihood of malignancy in a solitary pulmonary nodule. *Chest.* 1997;112:416–422.

24. Duhaylongsod FG, Lowe VJ, Patz EF Jr, Vaughn AL, Coleman RE, Wolfe WG. Detection of primary and recurrent lung cancer by means of F-18 fluorodeoxyglucose positron emission tomography (FDG PET). *J Thorac Cardiovasc Surg.* 1995;110:130–139.
25. Herder GJ, Golding RP, Gobar L, et al. The performance of 18-F-fluorodeoxyglucose positron emission tomography in small solitary pulmonary nodules. *Eur J Nucl Med Mol Imaging.* 2004;31:1231–1236.
26. Lowe VJ, Fletcher JW, et al. Prospective investigation of positron emission tomography in lung nodules. *J Clin Oncol.* 1998;16:1075–1084.
27. Lowe VJ, Hoffman JM, DeLong DM, Patz EF, Coleman RE. Semiquantitative and visual analysis of FDG-PET images in pulmonary abnormalities. *J Nucl Med.* 1994;35:1771–1776.
28. Nomori H, Watanabe K, Ohtsuka T, Naruke T, Suemasu K, Uno K. Visual and semiquantitative analyses for F-18 fluorodeoxyglucose PET scanning in pulmonary nodules 1 cm to 3 cm in size. *Ann Thorac Surg.* 2005;79:984–988.
29. Gugiatti A, Grimaldi A, Rossetti C, et al. Economic analyses on the use of positron emission tomography for the work-up of solitary pulmonary nodules and for staging patients with non-small-cell-lung-cancer in Italy. *Q J Nucl Med Mol Imaging.* 2004;48:49–61.
30. LeJeune C, Al Zahouri K, Woronoff-Lemsi MC, et al. Use of a decision analysis model to assess the medicoeconomic implications of FDG PET imaging in diagnosing a solitary pulmonary nodule. *Eur J Health Econ.* 2005; 6:203–214.
31. Henschke CI, Yankelevitz DF, Naidich DP, et al. CT screening for lung cancer: suspiciousness of nodules according to size on baseline scans. *Radiology.* 2004;231:164–168.
32. Bastarrika G, Garcia-Velloso MJ, Lozano MD, et al. Early lung cancer detection using spiral computed tomography and positron emission tomography. *Am J Respir Crit Care Med.* 2005;171:1378–1383.
33. Coleman RE, Laymon CM, Turkington TG. FDG imaging of lung nodules: a phantom study comparing SPECT, camera-based PET, and dedicated PET. *Radiology.* 1999;210:823–828.
34. Zhuang H, Pourdehnad M, Lambright ES, et al. Dual-time-point ^{18}F-FDG PET imaging for differentiating malignant from inflammatory processes. *J Nucl Med.* 2001;42:1412–1417.
35. Nakamoto Y, Higashi T, Sakahara H, et al. Delayed ^{18}F-FDG PET scan for the differentiation between malignant and benign lesions [abstract]. *J Nucl Med.* 1999;40(suppl):247P.
36. Matthies A, Hickeson M, Cuchiara A, Alavi A. Dual-time-point ^{18}F-FDG PET for the evaluation of pulmonary nodules. *J Nucl Med.* 2002;43:871–875.
37. Ponzo F, Zhuang HM, Liu FM, et al. Can the difference of the levels of glucose-6-phosphatase explain the mechanism of FDG-PET dual time point imaging? [abstract]. *Eur J Nucl Med.* 2001;28:OS399.
38. Higashi K, Ueda Y, Seki H, et al. Fluorine-18-FDG PET imaging is negative in bronchioloalveolar lung carcinoma. *J Nucl Med.* 1998;39:1016–1020.
39. Kim BT, Kim Y, Lee KS, et al. Localized form of bronchioloalveolar carcinoma: FDG PET findings. *AJR.* 1998;170:935–939.
40. Lee KS, Kim Y, Han J, Ko EJ, Park CK, Primack SL. Bronchioloalveolar carcinoma: clinical, histopathologic, and radiologic findings. *RadioGraphics.* 1997;17:1345–1357.
41. Heyneman LE, Patz EF. PET imaging in patients with bronchioloalveolar cell carcinoma. *Lung Cancer.* 2002;38:261–266.
42. Erasmus JJ, McAdams HP, Patz EF Jr, Coleman RE, Ahuja V, Goodman PC. Evaluation of primary pulmonary carcinoid tumors using positron emission tomography with 18-F-fluorodeoxyglucose. *AJR.* 1998;170:1369–1373.
43. Ahuja V, Coleman RE, Herndon J, Patz EF. The prognostic significance of fluorodeoxyglucose positron emission tomography imaging for patients with nonsmall cell lung carcinoma. *Cancer.* 1998;83:918–924.
44. Dhital K, Saunders CA, Seed PT, O'Doherty MJ, Dussek J. [(18)F] Fluorodeoxyglucose positron emission tomography and its prognostic value in lung cancer. *Eur J Cardiothorac Surg.* 2000;18:425–428.
45. Downey RJ, Akhurst T, Gonen M, et al. Preoperative F-18 fluorodeoxyglucose–positron emission tomography maximal standardized uptake value predicts survival after lung cancer resection. *J Clin Oncol.* 2004;22:3255–3260.
46. Ollenberger G, Knight S, Tauro A. False-positive FDG positron emission tomography in pulmonary amyloidosis. *Clin Nucl Med.* 2004;29: 657–658.
47. Shin L, Katz D, Yung E. Hypermetabolism on F-18 FDG PET of multiple pulmonary nodules resulting from bronchiolitis obliterans organizing pneumonia. *Clin Nucl Med.* 2004;29:654–656.
48. Cymbalista M, Weysberg A, Zacharius C, et al. CT demonstration of the 1996 AJCC-UICC regional lymph node classification for lung cancer staging. *RadioGraphics.* 1999;19:899–900.
49. Cerfolio RJ, Ojha B, Bryant AS, Bass CS, Bartalucci AA, Mountz JM. The role of FDG-PET scan in staging patients with non-small cell carcinoma. *Ann Thorac Surg.* 2003;76:861–866.
50. Platt JF, Glazer GM, Gross BH, Quint LE, Francis IR, Orringer MB. CT evaluation of mediastinal lymph nodes in lung cancer: influence of the lobar site of the primary neoplasm. *AJR.* 1987;149:683–686.
51. Mountain CF. The International System for Staging Lung Cancer. *Semin Surg Oncol.* 2000;18:106–115.
52. Herman SJ, Winton TL, Weisbrod GL, Towers MJ, Mentzer SJ. Mediastinal invasion by bronchogenic carcinoma: CT signs. *Radiology.* 1994;190:841–846.
53. Libshitz HI, McKenna RJ. Mediastinal lymph node size in lung cancer. *AJR.* 1984;143:715–718.
54. Vershackelen JA, Bogaert J, De Wever W. Computed tomography in staging for lung cancer. *Eur Respir J.* 2002;19(suppl):40S–48S.
55. Glazer GM, Gross BH, Quint LE, et al. Normal mediastinal lymph nodes: number and size according to American Thoracic Society mapping. *AJR.* 1985;144:261–265.
56. Shields TW. The significance of ipsilateral lymph node metastasis (N2 disease) in non small cell carcinoma of the lung: a commentary. *J Thorac Cardiovasc Surg.* 1990;99:48–53.
57. Quint LE, Francis IR, Wahl RL, et al. Preoperative staging of non-small-cell carcinoma of the lung: imaging methods. *AJR.* 1995;164:1349–1359.
58. Klein JS, Webb WR. The radiologic staging of lung cancer. *J Thorac Imaging.* 1991;7:29–47.
59. Sider L, Horejs D. Frequency of extrathoracic metastasis from bronchogenic carcinoma in patients with normal sized hilar and mediastinal lymph nodes on CT. *AJR.* 1988;151:893–895.
60. Stitik FP. Staging of lung cancer. *Radiol Clin North Am.* 1990;28:619–630.
61. Oliver TW, Bernadino ME, Miller JI, Mansour K, Greene D, Davis WA. Isolated adrenal masses in non small cell bronchogenic carcinoma. *Radiology.* 1984;153:217–218.
62. Sandler MA, Pearlberg JL, Madrazo BL, Gitschlag KF, Gross SC. Computed tomography evaluation of the adrenal gland in the preoperative assessment of bronchogenic carcinoma. *Radiology.* 1982;145:733–736.
63. Remer EM, Obuchowski N. Adrenal mass evaluation in patients with lung carcinoma: a cost-effectiveness analysis. *AJR.* 2000;174:1033–1039.
64. Mountain CF, Dressler CM. Regional lymph node classification for lung cancer staging. *Chest.* 1997;111:1718–1723.
65. van Tinteren H, Hoekstra OS, Smit EF, et al. Effectiveness of positron emission tomography in the preoperative assessment of patients with suspected non-small-cell lung cancer: the PLUS multicentre randomised trial. *Lancet.* 2002; 359:1388–1392.
66. Pieterman RM, van Putten JWG, Meuzelaar JJ, et al. Preoperative staging of non-small cell lung cancer with positron emission tomography. *N Engl J Med.* 2000;343:254–261.
67. Detterbeck FC, Falen S, Rivera MP, Halle JS, Socinski MA. Seeking a home for a PET, part 2: defining the appropriate place for positron emission tomography imaging in the staging of patients with suspected lung cancer. *Chest.* 2004; 125:2300–2308.
68. Detterbeck FC, Jones DR, Molina PL. Extrathoracic staging. In: Detterbeck FC, Rivera MP, Socinski MA, Rosenman JG, eds. *Diagnosis and Treatment of Lung Cancer: An Evidence-Based Guide for the Practicing Clinician.* Philadelphia, PA: W.B. Saunders; 2001:94–110.
69. Hatter J, Kohman LJ, Mosca RS, et al. Preoperative evaluation of stage I and stage II non-small cell lung cancer. *Ann Thorac Surg.* 1994;58:1738–1741.
70. Grant D, Edwards D, Goldstraw P. Computed tomography of the brain, chest, and abdomen in the postoperative assessment of non-small cell lung cancer. *Thorax.* 1988;43:883–886.
71. Staples CA, Muller NL, Miller RR, et al. Mediastinal nodes in bronchogenic carcinoma: comparison between CT and mediastinoscopy. *Radiology.* 1988; 167:367–372.
72. Detterbeck FC, Jones DR, Parker LA Jr. Intrathoracic staging. In: Detterbeck FC, Rivera MP, Socinski MA, et al., eds. *Diagnosis and Treatment of Lung Cancer: An Evidence Based Guide for the Practicing Clinician.* Philadelphia, PA: W.B. Saunders; 2001:73–93.
73. Dwamena BA, Sonnad SS, Angobaldo JO, Wahl RL. Metastases from non-small cell lung cancer: mediastinal staging in the 1990s—meta-analytic comparison of PET and CT. *Radiology.* 1999;213:530–536.
74. Lardinois D, Weder W, Hany TF, et al. Staging of non-small-cell lung cancer with integrated positron-emission tomography and computed tomography. *N Engl J Med.* 2003;348:2500–2507.
75. Halpern BS, Schiepers C, Weber WA, et al. Presurgical staging of non-small cell lung cancer: positron emission tomography, integrated positron emission tomography/CT, and software image fusion. *Chest.* 2005;128:2289–2297.

76. Antoch G, Stattaus J, Nemat AT, et al. Non–small cell lung cancer: dual-modality PET/CT in preoperative staging. *Radiology.* 2003;229:526–533.
77. Vansteenkiste J. FDG-PET for lymph node staging in NSCLC: a major step forward, but beware of the pitfalls. *Lung Cancer.* 2005;47:151–153.
78. Verhagen AF, Bootsma GP, Tjan-Heijnan VC, et al. FDG-PET in staging lung cancer: how does it change the algorithm? *Lung Cancer.* 2004;44:175–181.
79. Nomori H, Watanabe K, Ohtsuka T, Naruke T, Suemasu K, Uno K. The size of metastatic foci and lymph nodes yielding false-negative and false-positive lymph node staging with positron emission tomography in patients with lung cancer. *J Thorac Cardiovasc Surg.* 2004;127:1087–1092.
80. Takamochi K, Yoshida J, Murakami K, et al. Pitfalls in lymph node staging with positron emission tomography in non-small cell lung cancer patients. *Lung Cancer.* 2005;47:235–242.
81. Gonzalez-Stawinski GV, Lemaire A, Merchant F, et al. A comparative analysis of positron emission tomography and mediastinoscopy in staging non–small cell lung cancer. *J Thorac Cardiovasc Surg.* 2003;126:1900–1905.
82. Hicks RJ, Kalff V, MacManus MP, et al. The utility of ^{18}F-FDG PET for suspected recurrent non–small cell lung cancer after potentially curative therapy: impact on management and prognostic stratification. *J Nucl Med.* 2001;42:1605–1613.
83. Seltzer MA, Yap C, Silverman DH, et al. The impact of PET on the management of lung cancer: the referring physician's perspective. *J Nucl Med.* 2002;43:752–756.
84. Tucker R, Coel M, Ko J, Morris P, Druger G, McGuigan P. Impact of fluorine-18 fluorodeoxyglucose positron emission tomography on patient management: first year's experience in a clinical center. *J Clin Oncol.* 2001;19:2504–2508.
85. Kubota R, Kubota K, Yamada S, Tada M, Ido T, Tamahashi N. Microautoradiographic study for the differentiation of intratumoral macrophages, granulation tissues and cancer cells by the dynamics of fluorine-18-fluorodeoxyglucose uptake. *J Nucl Med.* 1994;35:104–112.
86. Vansteenkiste JF, Stroobants SG, De Leyn PR, et al. Lymph node staging in non-small-cell lung cancer with FDG-PET scan: a prospective study on 690 lymph node stations from 68 patients. *J Clin Oncol.* 1998;16:2142–2149.
87. Passlick B. Mediastinal staging (take home messages). *Lung Cancer.* 2004; 45(suppl 2):S85–S87.
88. Hollings N, Shaw P. Diagnostic imaging of lung cancer. *Eur Respir J.* 2002; 19:722–742.
89. Filderman AE, Shaw C, Matthay RA. Lung cancer, part I: etiology, pathology, natural history, manifestations, and diagnostic techniques. *Invest Radiol.* 1986;21:80–90.
90. Elias AD. Small cell lung cancer: state-of-the-art therapy in 1996. *Chest.* 1997;112(suppl):251S–258S.
91. Pearlberg JL, Sandler MA, Lewis JW Jr, Beute GH, Alpern MB. Small-cell bronchogenic carcinoma: CT evaluation. *AJR.* 1988;150:265–268.
92. Hansen M, Hansen HH, Dombernowsky P. Long-term survival in small cell carcinoma of the lung. *JAMA.* 1980;244:247–250.
93. Whitley NO, Fuks JZ, McCrea ES, et al. Computed tomography of the chest in small cell lung cancer: potential new prognostic signs. *AJR.* 1984;141:885–892.
94. Matthews MJ. Morphology of lung cancer. *Semin Oncol.* 1974;1:175–182.
95. Haque AK. Pathology of carcinoma of lung: an update on current concepts. *J Thorac Imaging.* 1991;7:9–20.
96. Abrams J, Doyle LA, Aisner J. Staging, prognostic factors, and special considerations in small cell lung cancer. *Semin Oncol.* 1988;15:261–277.
97. Detterbeck FC, Vansteenkiste JF, Morris DE, Dooms CA, Khandani AH, Socinski MA. Seeking a home for a PET, part 3: emerging applications of positron emission tomography imaging in the management of patients with lung cancer. *Chest.* 2004;126:1656–1666.
98. Blum R, MacManus MP, Rischin D, Michael M, Ball D, Hicks RJ. Impact of positron emission tomography on the management of patients with small-cell lung cancer: preliminary experience. *Am J Clin Oncol.* 2004;27:164–171.
99. Bradley JD, Dehdashti F, Mintun MA, Govindan R, Trinkaus K, Siegel BA. Positron emission tomography in limited-stage small-cell lung cancer: a prospective study. *J Clin Oncol.* 2004;22:3248–3254.
100. Brink I, Schumacher T, Mix M, et al. Impact of [^{18}F]FDG-PET on the primary staging of small-cell lung cancer. *Eur J Nucl Med Mol Imaging.* 2004;31:1614–1620.
101. Kamel EM, Zwahlen D, Wyss MT, Stumpe KD, von Schulthess GK, Steinert HC. Whole-body ^{18}F-FDG PET improves the management of patients with small cell lung cancer. *J Nucl Med.* 2003;44:1911–1917.
102. Weinstein M, Fineberg H. *Clinical Decision Analysis.* Philadelphia, PA: W.B. Saunders; 1980.
103. Scott WJ, Shepherd J, Gambhir SS. Cost-effectiveness of FDG-PET for staging non-small cell lung cancer: a decision analysis. *Ann Thorac Surg.* 1998;66: 1876–1883.
104. Gambhir SS, Hoh CK, Phelps ME, Madar I, Maddahi J. Decision tree sensitivity analysis for cost-effectiveness of FDG-PET in the staging and management of non–small-cell lung carcinoma. *J Nucl Med.* 1996;37:1428–1436.
105. Alzahouri K, LeJeune C, Woronoff-Lemsi MC, Arveux P, Guillemin F. Cost-effectiveness analysis of strategies introducing FDG-PET into the mediastinal staging of non-small-cell lung cancer from the French healthcare system perspective. *Clin Radiol.* 2005;60:479–492.
106. Sloka JS, Hollett PD, Mathews M. Cost-effectiveness of positron emission tomography for non-small cell lung carcinoma in Canada. *Med Sci Monit.* 2004;10:MT73–MT80.
107. Dietlein M, Weber K, Gandjour A, et al. Cost-effectiveness of FDG-PET for the management of potentially operable non-small cell lung cancer: priority for a PET-based strategy after nodal-negative CT results. *Eur J Nucl Med.* 2000;27: 1598–1609.
108. Pantel K, Izbicki J, Passlick B, et al. Frequency and prognostic significance of isolated tumour cells in bone marrow of patients with non-small cell lung cancer without overt metastases. *Lancet.* 1996;347:649–653.
109. Baum RP, Hellwig D, Mezzetti M. Position of nuclear medicine modalities in the diagnostic workup of cancer patients: lung cancer. *Q J Nucl Med Mol Imaging.* 2004;48:119–142.
110. MacManus MP, Hicks RJ, Matthews JP, et al. High rate of detection of unsuspected distant metastases by PET in apparent stage III non-small-cell lung cancer: implications for radical radiation therapy. *Int J Radiat Oncol Biol Phys.* 2001;50:287–293.
111. Oliver TW, Bernardino ME, Miller JI, et al. Isolated adrenal masses in non-small cell bronchogenic carcinoma. *Radiology.* 1984;153:217–218.
112. Ettinghausen SE, Burt ME. Prospective evaluation of unilateral adrenal masses in patients with operable non-small cell lung cancer. *J Clin Oncol.* 1991;9:1462–1466.
113. Erasmus JJ, Patz EF Jr, McAdams HP, et al. Evaluation of adrenal masses in patients with bronchogenic carcinoma using ^{18}F-fluorodeoxyglucose positron emission tomography. *AJR.* 1997;168:1357–1360.
114. Yun M, Kim W, Alnafisi N, Lacorte L, Jang S, Alavi A. ^{18}F-FDG PET in characterizing adrenal lesions detected on CT or MRI. *J Nucl Med.* 2001;42: 1795–1799.
115. Bury T, Barreto A, Daenen F, Barthelemy N, Ghaye B, Rigo P. Fluorine-18 deoxyglucose positron emission tomography for the detection of bone metastases in patients with non-small cell lung cancer. *Eur J Nucl Med.* 1998;25:1244–1247.
116. Gayed I, Vu T, Johnson M, Macapinlac H, Podoloff D. Comparison of bone and 2-deoxy-2-[^{18}F]fluoro-D-glucose positron emission tomography in the evaluation of bony metastases in lung cancer. *Mol Imaging Biol.* 2003;5:26–31.
117. Kao CH, Hsieh JF, Tsai SC, Ho YJ, Yen RF. Comparison and discrepancy of ^{18}F-2-deoxyglucose positron emission tomography and Tc-99m MDP bone scan to detect bone metastases. *Anticancer Res.* 2000;20:2189–2192.
118. Cheran SK, Herndon JE II, Patz EF Jr. Comparison of whole-body FDG-PET to bone scan for detection of bone metastases in patients with a new diagnosis of lung cancer. *Lung Cancer.* 2004;44:317–325.
119. Hsia TC, Shen YY, Yen RF, Kao CH, Changlai SP. Comparing whole body ^{18}F-2-deoxyglucose positron emission tomography and technetium-99m methylene diophosphate bone scan to detect bone metastases in patients with non-small cell lung cancer. *Neoplasma.* 2002;49:267–271.
120. Marom EM, McAdams HP, Erasmus JJ, et al. Staging non-small cell lung cancer with whole-body PET. *Radiology.* 1999;212:803–809.
121. Fogelman I, Cook G, Israel O, Van der Wall H. Positron emission tomography and bone metastases. *Semin Nucl Med.* 2005;35:135–142.
122. Abe K, Sasaki M, Kuwabara Y, et al. Comparison of ^{18}FDG-PET with ^{99m}Tc-HMDP scintigraphy for the detection of bone metastases in patients with breast cancer. *Ann Nucl Med.* 2005;19:573–579.
123. Ludwig V, Komori T, Kolb D, Martin WH, Sandler MP, Delbeke D. Cerebral lesions incidentally detected on 2-deoxy-2-[^{18}F]fluoro-D-glucose positron emission tomography images of patients evaluated for body malignancies. *Mol Imaging Biol.* 2002;4:359–362.
124. Therasse P, Arbuck SG, Eisenhauer EA, et al. New guidelines to evaluate the response to treatment in solid tumors. European Organization for Research and Treatment of Cancer, National Cancer Institute of the United States, National Cancer Institute of Canada. *J Natl Cancer Inst.* 2000;92:205–216.
125. Weber WA. Use of PET for monitoring cancer therapy and for predicting outcome. *J Nucl Med.* 2005;46:983–995.
126. Cerfolio RJ, Ojha B, Mukherjee S, et al. Positron emission tomography scanning with 2-fluoro-2-deoxy-d-glucose as a predictor of response of neoadjuvant treatment for non-small cell carcinoma. *J Thorac Cardiovasc Surg.* 2003;125:938–944.

127. Port JL, Kent MS, Korst RJ, et al. Positron emission tomography scanning poorly predicts response to preoperative chemotherapy in non-small cell lung cancer. *Ann Thorac Surg.* 2004;77:254–259.
128. Akhurst T, Downey RJ, Ginsberg MS, et al. An initial experience with FDG-PET in the imaging of residual disease after induction therapy for lung cancer. *Ann Thorac Surg.* 2002;73:259–266.
129. Choi NC, Fischman AJ, Niemierko A, et al. Dose-response relationship between probability of pathologic tumor control and glucose metabolic rate measured with FDG PET after preoperative chemoradiotherapy in locally advanced non-small-cell lung cancer. *Int J Radiat Oncol Biol Phys.* 2002;54: 1024–1035.
130. Weber WA, Petersen V, Schmidt B, et al. Positron emission tomography in non-small-cell lung cancer: prediction of response to chemotherapy by quantitative assessment of glucose use. *J Clin Oncol.* 2003;21:2651–2657.
131. Patz EF Jr, Connolly J, Herndon J. Prognostic value of thoracic FDG PET imaging after treatment for non-small cell lung cancer. *AJR.* 2000;174: 769–774.
132. Nestle U, Walter K, Schmidt S, et al. ^{18}F-Deoxyglucose positron emission tomography (FDG-PET) for the planning of radiotherapy in lung cancer: high impact in patients with atelectasis. *Int J Radiat Oncol Biol Phys.* 1999;44: 593–597.
133. Schmucking M, Baum RP, Griesinger F, et al. Molecular whole-body cancer staging using positron emission tomography: consequences for therapeutic management and metabolic radiation treatment planning. *Recent Results Cancer Res.* 2003;162:195–202.
134. Kalff V, Hicks RJ, MacManus MP, et al. Clinical impact of ^{18}F fluorodeoxyglucose positron emission tomography in patients with non-small-cell lung cancer: a prospective study. *J Clin Oncol.* 2001;19:111–118.
135. Vanuytsel LJ, Vansteenkiste JF, Stroobants SG, et al. The impact of (18)F-fluoro-2-deoxy-D-glucose positron emission tomography (FDG-PET) lymph node staging on the radiation treatment volumes in patients with non-small cell lung cancer. *Radiother Oncol.* 2000;55:317–324.
136. Hebert ME, Lowe VJ, Hoffman JM, et al. Positron emission tomography in the pretreatment evaluation and follow-up of non-small cell lung cancer patients treated with radiotherapy: preliminary findings. *Am J Clin Oncol.* 1996;19: 416–421.
137. Erdi YE, Macapinlac H, Rosenzweig KE, et al. Use of PET to monitor the response of lung cancer to radiation treatment. *Eur J Nucl Med.* 2000;27: 861–866.
138. Erasmus JJ, McAdams HP, Rossi SE, Goodman PC, Coleman RE, Patz EF. FDG PET of pleural effusions in patients with non–small cell lung cancer. *AJR.* 2000;175:245–249.
139. Schaffler GJ, Wolf G, Schoellnast H, et al. Non-small cell lung cancer: evaluation of pleural abnormalities on CT scans with ^{18}F FDG PET. *Radiology.* 2004;231:858–865.
140. The American Thoracic Society and The European Respiratory Society. Pretreatment evaluation of non-small-cell lung cancer. *Am J Respir Crit Care Med.* 1997;156:320–332.
141. Steinert HC, Santos Dellea MM, Burger C, Stahel R. Therapy response evaluation in malignant pleural mesothelioma with integrated PET-CT imaging. *Lung Cancer.* 2005;49(suppl 1):S33–S35.
142. Rusch VW, Godwin JD, Shuman WP. The role of computed tomography scanning in the initial assessment and follow-up of malignant pleural mesothelioma. *J Thorac Cardiovasc Surg.* 1988;96:171–177.
143. Benard F, Sterman D, Smith RJ, et al. Metabolic imaging of malignant pleural mesothelioma with fluorodeoxyglucose positron-emission tomography. *Chest.* 1998;114:713–722.
144. Schneider DB, Clary-Macy C, Challa S, et al. Positron-emission tomography with F18-fluorodeoxyglucose in the staging and preoperative evaluation of malignant pleural MPM. *J Thorac Cardiovasc Surg.* 2000;120:128–133.
145. Carretta A, Landoni C, Melloni G, et al. 18-FDG positron emission tomography in the evaluation of malignant pleural diseases: a pilot study. *Eur J Cardiothorac Surg.* 2000;17:377–383.
146. Buchmann I, Guhlmann CA, Elsner K, et al. F-18-FDG PET for primary diagnosis differential diagnosis of pleural processes [in German]. *Nuklearmedizin.* 1999;38:319–322.
147. Nanni C, Castellucci P, Farsad M, et al. Role of ^{18}F-FDG PET for evaluating malignant pleural mesothelioma. *Cancer Biother Radiopharm.* 2004;19:149–154.
148. Erasmus JJ, Truong MT, Smythe WR, et al. Integrated computed tomography-positron emission tomography in patients with potentially resectable malignant pleural mesothelioma: staging implications. *J Thorac Cardiovasc Surg.* 2005;129:1364–1370.
149. Flores RM. The role of PET in the surgical management of malignant pleural mesothelioma. *Lung Cancer.* 2005;49(suppl 1):S27–S32.
150. Ogawa M, Ishino S, Mukai T, et al. ^{18}F-FDG accumulation in atherosclerotic plaques: immunohistochemical and PET imaging study. *J Nucl Med.* 2004;45: 1245–1250.
151. Yun M, Yeh D, Araujo LI, Jang S, Newberg A, Alavi A. F-18 FDG uptake in large arteries: a new observation. *Clin Nucl Med.* 2001;26:314–319.
152. Lederman R, Raylman R, Fisher SJ, et al. Detection of atherosclerosis using a novel positron sensitive probe and 18-fluorodeoxyglucose (FDG). *Nucl Med Commun.* 2001;22:747–753.
153. Bakheet S, Amin T, Alia AG, Kuzo R, Powe J. F-18 FDG uptake in benign esophageal disease. *Clin Nucl Med.* 1999;24:995–997.
154. Patel P, Alibazoglu H, Ali A, Fordham E, LaMonica G. Normal thymic uptake of FDG on PET imaging. *Clin Nucl Med.* 1996;21:772–775.
155. Brink I, Reinhardt M, Hoegerle S, Altehoefer C, Moser E, Nitzsche EU. Increased metabolic activity in the thymus gland studied with ^{18}F-FDG PET: age dependency and frequency after chemotherapy. *J Nucl Med.* 2001;42:591–595.
156. Aydin A, Hickeson M, Yu JQ, Zhuang H, Alavi A. Demonstration of excessive metabolic activity of thoracic and abdominal muscles on FDG-PET in patients with chronic obstructive pulmonary disease. *Clin Nucl Med.* 2005;30:159–164.
157. Minn H, Nuutila P, Lindholm P, et al. In vivo effects of insulin on tumor and skeletal muscle glucose metabolism in patients with lymphoma. *Cancer.* 1994;73:1490–1498.
158. Truong MT, Erasmus JJ, Munden RF, et al. Focal FDG uptake in mediastinal brown fat mimicking malignancy: a potential pitfall resolved on PET/CT. *AJR.* 2004;183:1127–1132.
159. Shreve P, Anzai Y, Wahl RL. Pitfalls in oncologic diagnosis with FDG PET imaging: physiologic and benign variants. *RadioGraphics.* 1999;19:61–77.
160. Alavi A, Gupta N, Alberini JL, et al. Positron emission tomography imaging in nonmalignant thoracic disorders. *Semin Nucl Med.* 2002;32:293–321.
161. Yao W, Hoh C, Hawkins RA, et al. Quantitative PET imaging of bone marrow glucose metabolic response to hematopoietic cytokines. *J Nucl Med.* 1995;36:794–799.
162. Truong M, Erasmus JJ, Macapinlac HA, et al. Integrated PET/CT in patients with non small cell lung cancer: normal variants and pitfalls. *J Comput Assist Tomogr.* 2005;29:205–209.
163. Thie JA. Understanding the standardized uptake value, its methods, and implications for usage. *J Nucl Med.* 2004;45:1431–1434.
164. Boellaard R, Krak NC, Hoekstra OS, Lammertsma AA. Effects of noise, image resolution, and ROI definition on the accuracy of standard uptake values: a simulation study. *J Nucl Med.* 2004;45:1519–1527.
165. Geworski L, Knoop BO, de Cabrejas ML, Knapp WH, Munz DL. Recovery correction for quantitation in emission tomography: a feasibility study. *Eur J Nucl Med.* 2000;27:161–169.
166. Pan T, Mawlawi O, Nehmeh SA, et al. Tumor quantitation in the thorax with average CT and helical CT on PET/CT [abstract]. *J Nucl Med.* 2005; 46(suppl):108P.
167. Quon A, Napel S, Beaulieu C, Gambhir S. Novel 3D rendered FDG PET/CT virtual bronchoscopy and colonography for improved lesion localization and presurgical evaluation [abstract]. *J Nucl Med.* 2005;46(suppl):108P–109P.
168. Buck AK, Hetzel M, Schirrmeister H, et al. Clinical relevance of imaging proliferative activity in lung nodules. *Eur J Nucl Med Mol Imaging.* 2005;32:525–533.
169. Cobben DC, Elsinga PH, Hoekstra HJ, et al. Is ^{18}F-3′-Fluoro-3′-deoxy-L-thymidine useful for the staging and restaging of non–small cell lung cancer? *J Nucl Med.* 2004;45:1677–1682.
170. Tian M, Zhang H, Higuchi T, Oriuchi N, Endo K. Oncological diagnosis using (11)C-choline-positron emission tomography in comparison with 2-deoxy-2-[(18)F] fluoro-D-glucose-positron emission tomography. *Mol Imaging Biol.* 2004;6:172–179.